Ocean Engineering 283 (2023) 115353

Contents lists available at ScienceDirect

Ocean Engineering

journal homepage: www.elsevier.com/locate/oceaneng

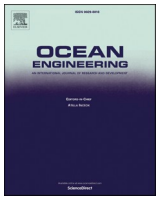

Development and validation of a parametric tropical cyclone wave height prediction model

Guisela Grossmann-Matheson [a], Ian R. Young [a,*], Jose-Henrique Alves [b], Alberto Meucci [a]

[a] Department of Infrastructure Engineering, University of Melbourne, Melbourne, Australia
[b] NOAA Research, Washington D.C., USA

ARTICLE INFO

Handling Editor: Prof. A.I. Incecik

ABSTRACT

A parametric model for computationally efficient wave height estimation within tropical cyclone conditions is developed. An updated wind vortex model is used to force a moving grid version of the WAVEWATCH III spectral model, to generate a large synthetic tropical cyclone wave field database (approximately 400 simulations). This extensive database is used to develop the parametric model which accounts for the key variables defining the magnitude and spatial distribution of waves within tropical cyclones. The model uses JONSWAP-type scaling and accounts for the effects of the moving vortex of the tropical cyclone in defining the wave field. A total of 28 buoy observations together with satellite altimeters measurements during the passage of 17 tropical cyclones (hurricanes) in the North Atlantic Ocean and Gulf of Mexico were used to validate the predicted wave heights. The resulting model is computationally efficient, making it ideal for engineering applications which require simulation of numerous tropical cyclone cases. Despite some limitations, it is a useful tool for the prediction of wave heights under extreme tropical cyclone forcing.

1. Introduction

Waves generated by tropical cyclones (TCs, hurricanes or typhoons) can cause damage to offshore structures and coastal settlements and play an important role in the design criteria for engineering projects such as ports, harbors, renewable energy facilities and in coastal risk assessment. There is also scientific interest in TC waves, as they may impact coupled ocean-atmosphere systems by modifying the air-sea fluxes and near surface turbulent processes (Doyle, 2002; Lee and Chen, 2012; Zhao et al., 2017; Garg et al., 2018; Varlas et al., 2020).

Accurate estimates of significant wave height within the extreme conditions of TCs generally require detailed estimates of the TC wind field and application of a third-generation spectral wave model (The WAMDI Group, 1988; Cardone et al., 1996; Alves et al., 2004). Although such applications have been shown to produce reliable results (e.g. Tolman et al., 2005; Liu et al., 2017; Zieger et al., 2021a), they come at significant computational cost (Zieger et al., 2015, 2021b).

Over the past 30 years, a range of studies have investigated the wave field within tropical cyclones. These studies include data from in situ buoys (e.g. Ochi, 1993; Young, 1988; 2006; Chao et al., 2005; Tolman et al., 2005; Moon et al., 2003; Fan et al., 2009; Hu and Chen, 2011; Alves et al., 2015; Liu et al., 2017; Collins et al., 2018; Tamizi and Young, 2020), aircraft-borne synthetic aperture radars (e.g. Black et al., 2007; Zhang et al., 2018), scanning radar altimeters (e.g. Wright et al., 2001, 2002, 2021; Moon et al., 2003; Fan et al., 2009; Hwang and Fan, 2017; Liu et al., 2017), satellite altimeters (e.g. Young and Burchell, 1996; Moon et al., 2003; Young and Vinoth, 2013; Liu et al., 2017; Tamizi and Young, 2020; Collins et al., 2021) and the application of spectral wave models (e.g. Tolman and Alves, 2005; Babanin et al., 2007; Hu et al., 2020; Tamizi et al., 2021; Beyramzadeh and Siadatmousavi, 2022; Yang et al., 2022).

A significant challenge in the accurate modelling of tropical cyclone wave fields is posed by the relatively small spatial extent of such systems. The spatial scale of TCs is often represented by the radius to maximum winds, R_{max}, with the maximum sustainable winds, V_{max} occurring close to the eyewall of the storm. Defining realistic TC wind fields requires high-resolution atmospheric model simulations (e.g. Strachan et al., 2013; Wehner et al., 2014; Haarsma et al., 2016; Roberts et al., 2020). Global wind reanalysis models, such as ERA5 produced by the European Center for Medium-Range Weather Forecasts (ECMWF; Hersbach et al., 2020) or the Climate Forecast System Reanalysis (CFSR; Saha et al., 2010), with a spatial resolution of approximately 25 km do

* Corresponding author.
E-mail address: ian.young@unimelb.edu.au (I.R. Young).

https://doi.org/10.1016/j.oceaneng.2023.115353
Received 19 May 2023; Received in revised form 24 June 2023; Accepted 8 July 2023
Available online 21 July 2023

not adequately resolve tropical cyclones (Campos et al., 2022).

Therefore, state-of-the-art modelling of tropical cyclone wave fields involves the use of high-resolution atmospheric circulation models, such as the hindcast model Oceanweather Inc. (OWI; Cox et al., 1995; Cardone and Cox, 2009) and the forecast model Hurricane Weather Research and Forecasting (HWRF; Biswas et al., 2018) to force high-resolution spectral wave models (Abdolali et al., 2020). Such spectral wave models are an important tool in producing reliable wave fields, as shown by Tolman and Alves (2005). For many applications, however, the computational cost of such an approach is not warranted. Such applications include extreme value analyses, which require the modelling of a long history of tropical cyclone events and climatological studies, in which tropical cyclone activity in a region over many years is required. In such applications, parametric models which represent the TC wind and wave fields in terms of a small number of parameters describing the meteorological characteristics of the TC have provided useful (Young, 2017). The apparent success of such models lies in the fact that they are not purely empirical. Rather, they rely on the observational evidence that the well-formed wind fields of mature TCs can be represented by vortex models and that an equivalent fetch can be defined for TCs as a function of the translation speed and the maximum wind velocity of the TC (Shemdin, 1977; King and Shemdin, 1978; Young, 1988). In addition, as nonlinear wave-wave interactions play a dominant role in defining the spectral form of TC waves, fetch-limited (JONSWAP-type) scaling can be used to define the wave field (Young, 2017; Hwang and Fan, 2017; Tamizi et al., 2021).

For such models to be reliable, however, they require a relatively large database to define the equivalent fetch, which is a function of multiple TC wind field parameters (velocity of forward movement, maximum wind speed, spatial scale of the storm). Observations from in situ measurements (Young, 1988; Bowyer and MacAfee, 2005) and satellite altimeters (Young and Burchell, 1996; Young and Vinoth, 2013) provide some insight but are generally too sparse to define the multi-parameter relationship between the equivalent fetch and the TC wind-field parameters. To address such deficiencies, spectral wave model data have been used to augment or replace the available observational data (Young, 1988). The success of such synthetic datasets relies on the sophistication of the spectral wave model used. To date, either the available model datasets have been generated by relatively simple models (Young, 1988), or have used more advanced simulations with a limited range of forcing conditions, yielding preliminary results (Alves et al., 2004).

This paper aims to address these limitations by developing a parametric TC wave height prediction model, based on data generated by numerous simulations with a validated moving grid implementation of the WAVEWATCH III (WW3) spectral wave model (WW3DG, 2019).

This paper is structured as follows. Section 2 describes the development of an updated wind vortex model for TCs to be used as the forcing wind field for the subsequent generation of a wave field database. Section 3 describes the generation and validation of the comprehensive synthetic TC wave field database using the WW3 spectral wave model. This database is used to develop the parametric wave height model, described and validated in Section 4. Conclusions are provided in Section 5.

2. Wind vortex model for tropical cyclones

Tropical cyclone wind field models typically have an axisymmetric vortex structure, with all radial distances in the wind profiles expressed as multiples of R_{max} and all velocities related to the maximum wind speed, V_{max} (Shapiro and Willoughby, 1982). For an axisymmetric vortex translating in a uniform flow, there is an azimuthal wavenumber asymmetry in the Earth-relative frame. This means that, at ground level, the strongest earth-relative winds lie to the right (Northern Hemisphere) of the translation vector, where the ambient winds reinforce those due to the vortex. In the Southern Hemisphere, the opposite occurs, with the strongest winds to the left of the storm track (Shapiro, 1983; Thomsen et al., 2015).

There are a range of parametric surface wind field models which have been proposed for TCs (e.g. Holland, 1980; Emanuel, 1986; Willoughby et al., 2006; Holland et al., 2010). Various studies have compared wind profiles obtained for different parametric wind models. Ruiz-Salcines et al. (2019) tested and evaluated six different parametric wind models, including Holland and Emanuel models, and found that a particular model may best represent a specific event, but when dealing with a large number of events, the choice of a particular parametric wind model cannot guarantee high levels of accuracy. This finding is consistent with Krien et al. (2018) who compare the performance of seven traditional wind fields empirical approaches and found none of them represented the best option in all cases. Rather, the choice of a particular parametric model depends on several criteria, such as TC intensity and the availability of reliable wind radii information.

Kalourazi et al. (2021) evaluated the most common parametric wind field models for TCs for the Gulf of Mexico storms and concluded that the Holland et al. (2010) model produced the best agreement with observations. Although Holland et al. (2010) has been extensively used to determine the surface (10m) wind speed, like other vortex models, it has a limitation since the resulting vortex is not embedded in any background flow. As a result, such models tend to underestimate observed winds at large values of radial distance (r) from the TC center (Young, 2017). To address such limitations, a number of approaches have been considered, including the use of a double vortex and embedding the TC vortex within a synoptic background flow (McConochie et al., 2004). Zieger et al. (2021a) performed a series of TC hindcast simulations using the parametric formulation proposed by Willoughby et al. (2006). They adjusted parameters, such as V_{max}, R_{max} and the radius to gales or 34 knots wind radii, R_{34} to fit the past storm profiles to a best track database. They then applied the dynamic three-dimensional Kepert-Wang model (Kepert and Wang, 2001; Kepert, 2012) to chosen Willoughby profiles and generated wind fields. These vortex wind fields were blended with ERA-Interim background wind fields and showed very good agreement between the model and the observed wind speeds. This approach, blending background winds to the parametric model used by Zieger et al. (2021a) has been used in other studies and demonstrated good results (Shao et al., 2018).

It should also be noted that the Holland et al. (2010) model uses two radii values to define the spatial extent of the TC vortex (radius to maximum winds, R_{max} and radius to gales, R_{34}, which results in greater skill in defining wind velocities at large values of r (Young, 2017) compared to models with a single radial scale (Holland, 1980).

The Holland vortex does not account for asymmetry of the wind field or any inflow angle. Shea and Gray (1973) studied the hurricane's inner core region and found a range of inflow angles with a mean of approximately 20°. Young (2017) assumed a constant inflow angle fixed of 25°. Other studies found a mean inflow angle of approximately 22° (Powell, 1982; Zhang and Uhlhorn, 2012; Tamizi et al., 2020).

Tamizi et al. (2020) used a 30-year multi-mission scatterometer dataset calibrated and validated by Ribal and Young (2020) to investigate TC wind inflow angle and asymmetry. They found that the maximum observed inflow angle (approximately 35°) occurred in the right rear quadrant (relative to the storm direction of movement), whilst the minimum inflow angle (approximately 10°) was found in the left front quadrant. They also observed that as the velocity of forward movement, V_{fm}, increases the inflow angle decreases ahead of the storm and increases behind the storm. In addition to the dependence on V_{fm} they observed that the inflow angle is a function of the distance from the storm center, (r). Their data indicated there was only a weak dependence of the inflow angle on the storm's central pressure, p_0.

For the present application, the inflow angle data of Tamizi et al. (2020) was parameterized as a cosine distribution as defined by equation (1).

$$\theta = a\cos(\beta + \varphi + \theta_{fm}) + b \tag{1}$$

where, θ is the inflow angle and a is a function of V_{fm} , defined by equation (2),

$$a = 5 + V_{fm} \tag{2}$$

All angles in (1) are measured counterclockwise from the x axis (mathematical convention). β is the angle defining the location where the inflow angle is being calculated, $\varphi = 75^0$ ensures the maximum inflow angle is in the right-rear quadrant (Tamizi et al., 2020) and θ_{fm} is the direction of propagation of the TC. The value b is a function of non-dimensional distance from the storm center defined by equation (3) as follows,

$$b = 0.3\frac{r}{R_{max}} + 19 \tag{3}$$

where r is the radial distance from the storm center to the location where the inflow angle is being calculated and R_{max} is the radius of maximum winds. All quantities in (1) have units of [degrees] and V_{fm} in (2) has units of [m/s].

Fig. 1 shows the parameterized inflow angle in a TC as a function of V_{fm}. These results are consistent with the Tamizi et al. (2020) (see their Fig. 14) observational data - the inflow angle is a maximum in the right-rear quadrant and a minimum in the left-front quadrant, with this variation increasing with V_{fm}. Note that all angles are referenced to the stationary Earth's surface (i.e., not in a frame of references moving with the TC).

Numerous studies have considered TC asymmetry, showing that this is, to first order, related to the velocity of forward movement (Shapiro, 1983; Holland, 2008; Hu et al., 2012; Uhlhorn et al., 2014; Klotz and Jiang, 2016; Olfateh et al., 2017; Tamizi et al., 2020). Tamizi et al. (2020) showed that the asymmetry can be approximated by the vector addition of $V_{fm}/2$ to the symmetric wind field vortex. For the present application, the vector addition of $V_{fm}/2$ is used to approximate the left-right wind field asymmetry. Note that the maximum wind velocity in the Holland et al. (2010) vortex already accounts for the velocity of forward movement through the B parameter of this model. Therefore, so as not to include the impact of the translation speed twice, the maximum wind velocity of the symmetric Holland et al. (2010) vortex was reduced by $V_{fm}/2$ before the vector addition of this component to all wind field locations.

2.1. Validation of the parametric tropical cyclone wind field

The parametric wind field model described above is clearly a considerable simplification of the two-dimensional structure of a TC. However, for typical applications of the subsequent parametric wave model, this level of complexity is believed appropriate. These applications will typically see the TC defined by parameters obtained from "best track" databases (e.g. IBTrACS, Knapp et al., 2010) and used in applications where many realizations of TC wave fields are required (e.g. climatology, extreme value analysis etc.). Therefore, for validation purposes, the aim is to determine if the wind field model can reproduce the broad features of historical storms. We hence choose as our

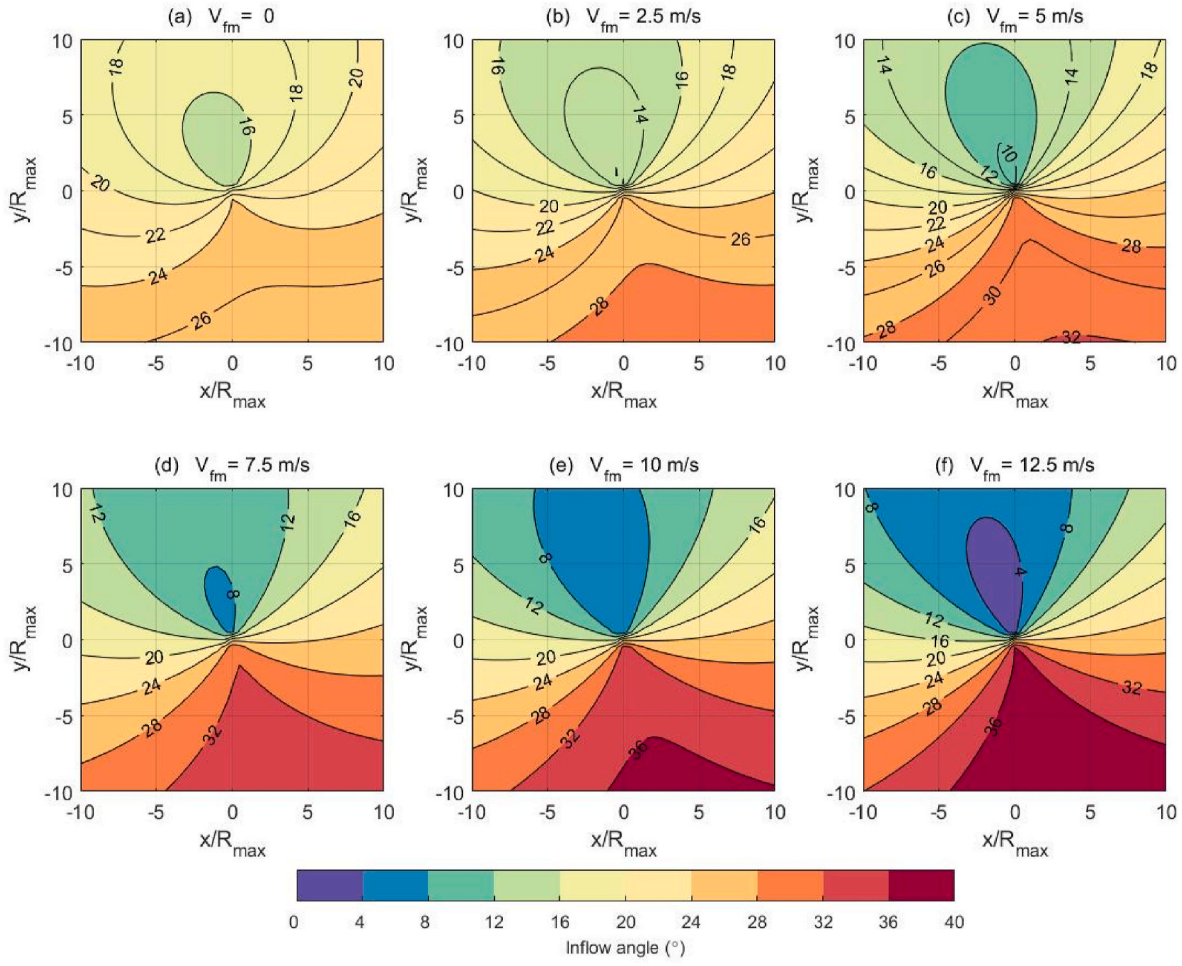

Fig. 1. Contours of wind inflow angle (degrees) obtained from the parametric relationship (1). Values are shown for velocities of forward movement: (a) $V_{fm} = 0$; (b) $V_{fm} = 2.5$ m/s; (c) $V_{fm} = 5$ m/s; (d) $V_{fm} = 7.5$ m/s; (e) $V_{fm} = 10$ m/s; (f) $V_{fm} = 12.5$ m/s. The tropical cyclone is propagating northward (up the page).

validation ("truth"), the NOAA Hurricane Research Division (HRD) Real-time Hurricane Wind Analysis System (H*Wind) post storm reanalysis dataset (Powell et al., 1998). Eight well documented historical hurricanes which formed in the northern Atlantic with tracks through both the Gulf of Mexico (Ivan, Katrina, Rita, Gustav and Ike) and towards the east coast of the United States (Earl, Irene and Matthew) were used to test the performance of the parametric wind field model (see Table A1). The TC wind field parameters from IBTrACS (International Best Track Archive for Climate Stewardship; Knapp et al., 2010) were used to define the parametric wind field model for each hurricane. IBTrACS represents the best estimate of TC parameters collected by 12 agencies around the world and provides: date, location, central pressure, p_0, radius to maximum winds, R_{max} and radius to gales, R_{34} for each TC. The velocity of forward movement, V_{fm} and direction of propagation, θ_{fm} were estimated from successive 3 hourly locations within the database. The central pressure drop, Δp was estimated from values of p_0 and an assumption of an ambient atmospheric pressure far from the TC of $p_{amb} = 1008$ hPa.

Typical comparisons of the H*Wind and parametric wind field models are shown in Figure A1 of the Appendix. The parameterized vortex model showed significant skill in reproducing the TC wind fields, noting the simplifications of such a vortex model and the accuracy of the IBTrACS parameters (Tamizi et al., 2020). Differences between the parametric vortex model and H*Wind maximum wind velocities are typically less than 10% (see Table A1), with the parametric vortex model showing an overall positive bias of 1.7% compared to the H*Wind reanalysis.

3. Synthetic tropical cyclone wave field database

Our aim is to generate a synthetic TC wave field database by successive runs of the WW3 spectral wave model. These runs will cover a broad range of TC parameters. As an initial step, however, we need to validate the WW3 configuration to be used when forced with the above parametric TC wind field.

3.1. Validation of WW3 wave field generated with parametric wind field forcing

As validation of the WW3 (WW3DG, 2019) implementation, we consider the same eight U.S. hurricanes used for the validation of the wind field in Section 2.1. WW3 has been extensively used to study surface wave dynamics, and as an operational wave model. It is a wind-wave modelling framework with alternative formulations for the physics of wind input and dissipation. WW3 has also been used in tropical cyclone investigations and is the underlying workhorse for hurricane wave forecasting at the US National Weather Service (Chao et al., 2005; Alves et al., 2015). It is under continuing development at NOAA/NCEP (Tolman, 1997, 1999a, 2002b, 2009, 2010a, 2014; WW3DG, 2016; 2019) along with contributors in the WAVEWATCH III Development Group (WW3DG). Version 6.07 was used for this study. The source term (physics) package used here is termed ST4 (Ardhuin et al., 2010). A detailed discussion of the settings used for this package, the rationale for its choice and alternative descriptions of the physics can be found in Section 3.1.3.

A high-resolution 0.05° grid was developed for the region 5°N to 40°N and 100°W to 60°W. Information on the bathymetry, sub-grid obstructions and a land-sea mask were generated using the software Gridgen v3.0 (Chawla and Tolman, 2007), which is part of the WW3 distribution. The software uses a high-resolution shoreline database (GSHHS - Global Self-consistent Hierarchical High-resolution Shoreline; Wessel and Smith, 1996) and it was modified to use the 15 arc seconds GEBCO bathymetry (General Bathymetric Chart of the Oceans; GEBCO, 2020), instead of default bathymetry (ETOPO 1; Amante and Eakins, 2009).

The bulk wave parameters: significant wave height (H_s), peak wave frequency (f_p), mean wave direction (θ_m) and peak wave direction (θ_p), together with the directional wave energy spectrum and the source terms were output for validation purposes. Where applicable, model quantities were validated against NOAA National Data Buoy Center (NDBC) data. The maximum values of significant wave height recorded at each NDBC buoy (H_s^{buoy}), together with the corresponding value simulated by WW3 (H_s^{WW3}) at these same buoy locations are shown on Table 1. The results show reasonable agreement between the measured data and the WW3 simulations using the parametric wind fields from the updated Holland model. Values of bias ($Bias^{WW3} = H_s^{WW3} - H_s^{buoy}$) are typically less than 10% of the buoy significant wave height (maximum bias is +19.1% for Hurricane Rita), with an overall small negative bias of −1.2% (WW3 lower than buoys). The RMSE is 1.17 m. Note that the parameters used to define the wind fields were taken from the IBTrACS dataset, with no attempt to optimize the wind fields or track information.

The results add confidence that the WW3 model forced with the parametric TC wind field model and using IBTrACS TC parameters can reproduce significant wave heights with reasonable accuracy. Further details of the validations for Hurricanes Ivan and Earl are provided below, to better understand WW3 performance.

3.1.1. Case 1: Hurricane Ivan

Hurricane Ivan crossed the Caribbean Sea and the Gulf of Mexico in September 2004 and reached Saffir–Simpson hurricane intensity scale (SSHS) category 5 strength, with a minimum central pressure of 910 hPa. Fig. 2a shows the parametric TC model wind field for the storm on September 15, 2004 at 00:00 UTC. The figure also shows the locations of NDBC buoys. Fig. 2 b, c and d show time series comparing values of H_s from buoys and the WW3 model. The WW3 model generally underestimates the maximum values of H_s at all three buoys, as indicated in Table 1, however, there is still an overall reasonable agreement between buoy and WW3 model data.

NDBC buoys 42001 and 42003 were closest to the hurricane track with spectral data available. Fig. 3 shows spectra when the eye of Hurricane Ivan was located southeast of Buoy 42001 and southwest of Buoy 42003 on 15 September of 2004 at 00:00 UTC (location shown in Fig. 2a). At the location of Buoy 42001, the wave direction is towards the northwest for both the buoy data (Fig. 3a) and WW3 results (Fig. 3c). The directional spectrum of Buoy 42003 (Fig. 3b) shows the wave direction towards the northwest. In contrast, the WW3 result (Fig. 3d) shows a peak corresponding to waves propagating to the north, with a broad directional spread covering waves propagating to the northwest (as shown by the buoy). Note that the WW3 model produces broader directional spreading than the buoy data. This is a well-known limitation of the Discrete Interaction Approximation (DIA) used to represent the nonlinear source term in the model (Hasselmann and Hasselmann, 1985; Banner and Young, 1994). The peak wave frequency, f_p measured by both buoys is 0.0725 Hz in reasonable agreement with the WW3 model results (0.0615 Hz), noting the challenges in measuring this parameter accurately (WW3 is 15% lower).

3.1.2. Case 2: Hurricane Earl

Hurricane Earl crossed the western part of the North Atlantic in late August and early September 2010 and reached SSHS category 4 strength at its peak, with a minimum central pressure of 927 hPa and maximum winds of ~64 m/s. As shown in Fig. 4, WW3 underestimates the maximum values of H_s at NDBC buoys 41001 and 41046 and overestimates at buoy 41043 (Table 1 and Fig. 4b and c and d). Overall, however, the results are in good agreement between buoys and WW3 model. At buoy 41046, the eye of the TC passes over buoy and both the model and buoy show a comparable decrease in H_s in the eye of the TC.

The validation results in Table 1 and Figs. 2–4 show that the WW3 model, forced with the parametric wind field model defined by IBTrACS

Table 1
Values of maximum significant wave height at buoy locations, H_s^{buoy} and the corresponding maximum values at those locations from the WW3 model, H_s^{WW3} and the parametric model H_s^{PModel} for eight U.S. hurricanes. Values of bias for the WW3 model, $Bias^{WW3} = H_s^{WW3} - H_s^{buoy}$ and for the parametric wave model $Bias^{PModel} = H_s^{PModel} - H_s^{buoy}$ are also show. The parametric wave model results (column 7) are discussed in section 4.1. Buoys with (*) are located in finite depth regions.

Hurricane	Year	NDBC buoy	H_s^{buoy}(m)	H_s^{WW3}(m)	$Bias^{WW3}$(m)	H_s^{PModel}(m)	$Bias^{PModel}$(m)
Ivan	2004	42001	8.77	7.29	−1.48	7.72	−1.05
		42003	11.04	9.82	−1.22	11.76	0.72
		42040	15.96	13.68	−2.28	15.58	−0.38
Katrina	2005	42003	10.57	11.25	0.68	13.48	2.91
Rita	2005	42019	5.92	4.87	−1.05	6.01	0.09
		42001	11.10	13.22	2.12	12.99	1.89
Gustav	2008	42001	5.48	5.25	−0.23	6.38	0.90
		42003	10.34	9.85	−0.49	12.20	1.86
		42040	10.32	9.58	−0.74	12.10	1.78
Ike	2008	41046	6.46	6.49	0.03	7.14	0.68
		42001	9.25	10.33	1.08	10.89	1.64
		42035*	6.03	5.67	−0.36	9.28	3.25
Earl	2010	41001	11.98	10.98	−1.00	13.30	1.32
		41043	9.41	9.90	0.49	11.45	2.04
		41046	14.81	13.20	−1.61	16.22	1.41
Irene	2011	41010	9.63	11.22	1.59	10.01	0.38
		41036*	8.64	9.92	1.28	12.04	3.40
Matthew	2016	41009*	9.07	9.96	0.89	13.00	3.93
		42058	10.35	9.73	−0.62	12.15	1.80
Edouard	1996	44004	10.98	–	–	9.78	−1.20
Floyd	1999	41010	15.50	–	–	15.10	−0.40
Lili	2002	42001	11.20	–	–	13.80	2.60
Wilma	2005	42056	11.00	–	–	12.03	1.03
Dean	2007	41040	8.09	–	–	9.29	1.20
Sandy	2012	41002	7.13	–	–	8.29	1.16
Joaquin	2015	41047	7.56	–	–	8.50	0.94
Maria	2017	41047	11.77	–	–	11.91	0.14
Sam	2021	41040	4.06	–	–	5.32	1.26

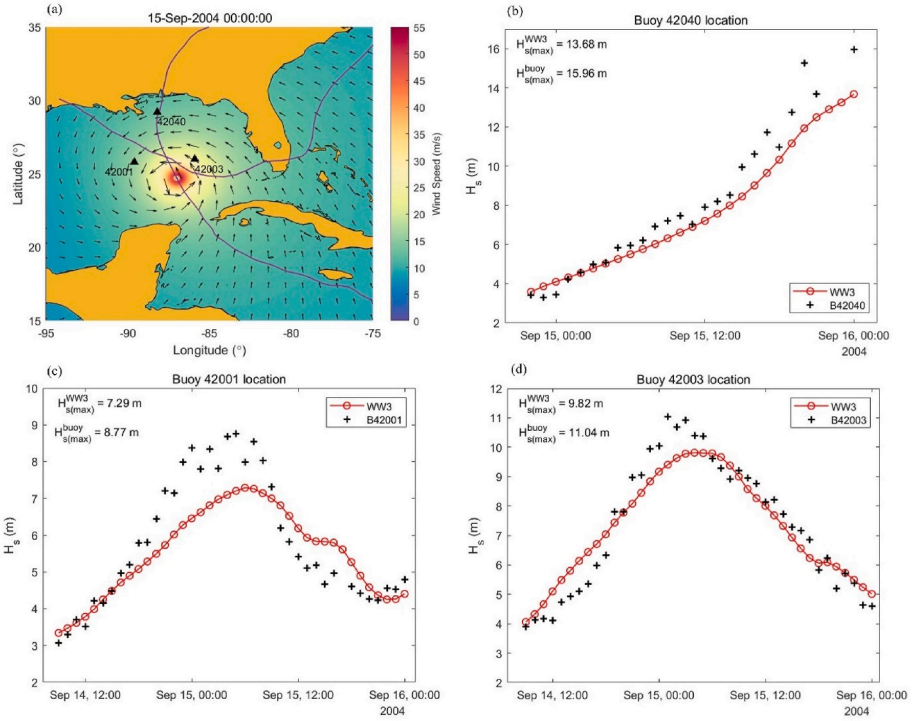

Fig. 2. (a) Wind field for Hurricane Ivan on 15 September of 2004 at 00:00 UTC (velocity contours in [m/s] and vector direction not scaled). (b), (c) and (d): H_s comparison between WW3 model and buoys 42040, 42001 and 42003 respectively.

parameters, produces largely unbiased values of significant wave height in reasonable agreement with buoy data.

3.1.3. Selection of WW3 source term package

The source/sink terms within the WW3 spectral model represent, for deep water, the physical processes of atmospheric input from the wind, nonlinear white-cap dissipation, nonlinear wave-wave

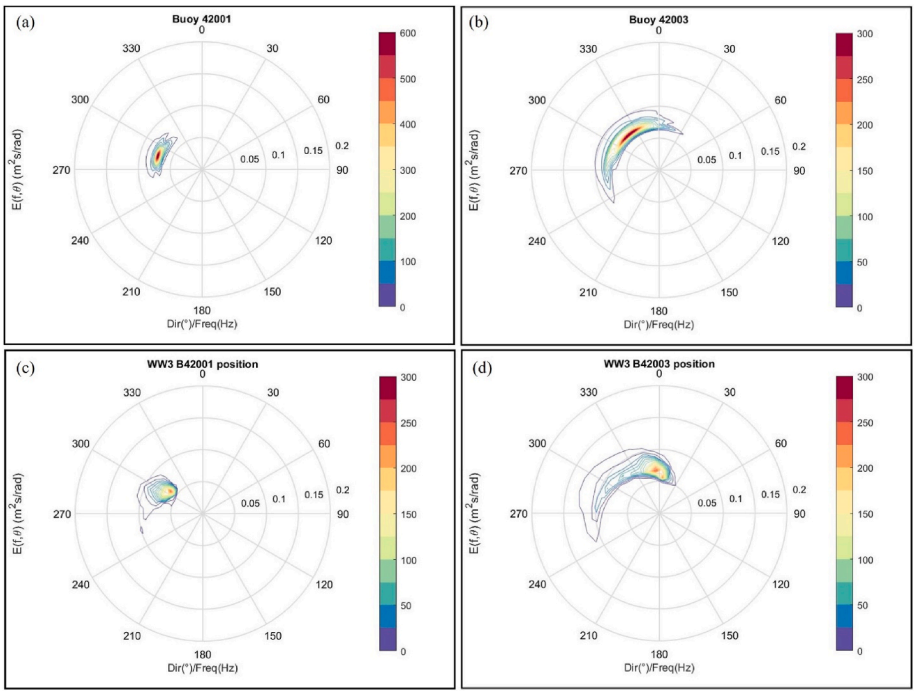

Fig. 3. Hurricane Ivan directional spectra on 15 September of 2004 at 00:00 UTC. On the left (a): Directional spectrum measured by Buoy 42001, and (c): Directional spectrum from WW3 at the position of Buoy 42001. On the right (b): Directional spectrum measured by Buoy 42003 and d: Directional spectrum from WW3 at the position of Buoy 42003.

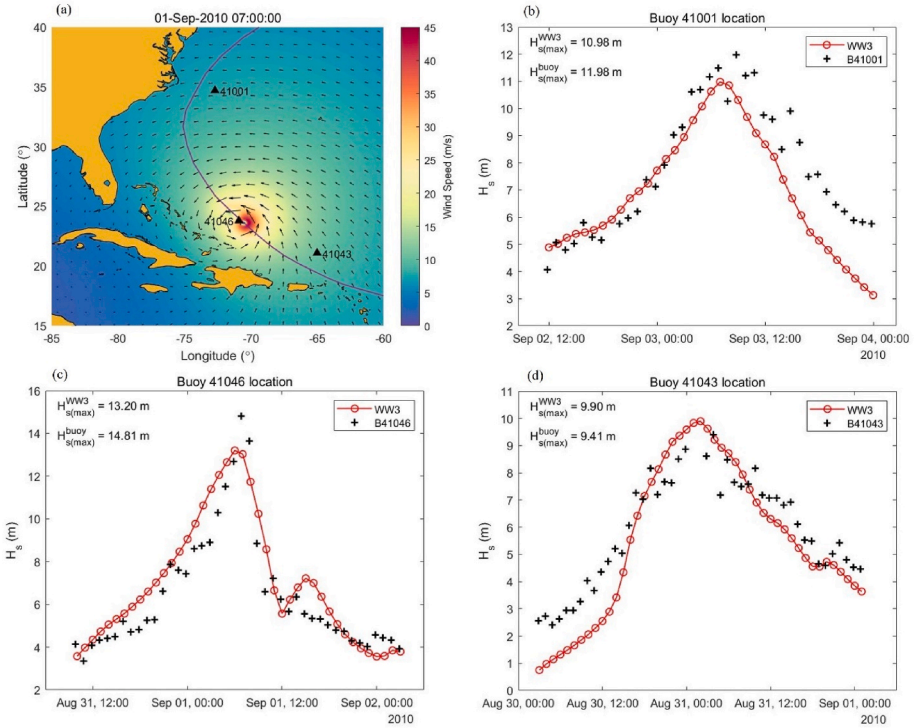

Fig. 4. (a): Wind field for Hurricane Earl on 01 September of 2010 at 07:00 UTC (velocity contours in [m/s], and wind direction not scaled). (b), (c) and (d): H_s comparison between WW3 model and buoys 41001, 41046 and 41043, respectively.

interaction, and swell decay.

Various source term packages (ST) have been proposed and implemented in WW3. These include: ST2 (Tolman and Chalikov, 1996), ST3 (Janssen, 1991; Bidlot et al., 2007; Bidlot, 2012), ST4 (Ardhuin et al. 2009, 2010; Rascle and Ardhuin, 2013; Leckler et al., 2013) and ST6 (Babanin and Young, 2005; Donelan et al., 2006; Young and Babanin, 2006; Babanin et al., 2007; Babanin, 2011; Rogers et al., 2012; Zieger et al., 2015; Liu et al., 2019).

A number of studies have evaluated the performance of WW3 under extreme weather conditions, such as TCs, using these different source

term packages. Liu et al. (2017) compared four source term packages for WW3 (ST2/3/4/6) and, with the exception of the older parameterization ST2, they found comparable performance of the other packages in terms of wave prediction. However, they found that all three tend to overestimate the energy of waves traveling in oblique and opposing winds. Zieger et al. (2015) made a comparative study between ST2, ST4 and ST6 and found that wave heights estimated with ST6 are slightly larger than the other packages. Bi et al. (2015) showed that for the Pacific Ocean, the ST4 package performs well in terms of overall wave parameters and that the ST6 package is slightly better in determining swell propagation/dissipation. Stopa et al. (2016) compared the four packages for global-scale applications and found that the ST4 and ST6 packages perform similarly and better than ST2 and ST3. They found that for all sea states ST4 has the lowest H_s biases and ST6 generally produces more accurate swell heights, due to stronger dissipation of swells, especially far from the storms. They also suggested that ST6 was inclined to overestimate the energy level of the high-frequency tail of the spectrum. Liu et al. (2019) subsequently recalibrated a number of the terms in the ST6 package, to address this issue.

Kalourazi et al. (2021) made comparisons between model results and in-situ observations during the passage of Hurricane Ivan (2004) and showed that a calibrated ST6 variant produced better results for simulating bulk wave parameters at locations under hurricane wind forcing. However, for areas beyond active forcing, and during fair weather conditions, a calibrated ST4 formulation was recommended. They also found that both formulations overestimate waves propagating in oblique and opposing winds, consistent with previous reports by Liu et al. (2017).

Zieger et al. (2021a) conducted a series of simulations of past storms for the northwest shelf region of Australia and found that, whilst the ST6 source term package performed well overall, there is no single configuration that performed best for all TCs evaluated. Abdolali et al. (2021) performed a validation study comparing atmospheric and wave model results with satellite altimeter and buoy data showing that uncertainties and errors embedded in atmospheric models are propagated to the wave model results. This point has also been identified by other authors (e.g., Tolman and Alves, 2005).

Soran et al. (2022) reported that a calibrated ST6 implementation had the best performance in extreme wave simulation in the Black Sea. The recent study by Yang et al. (2022) analyzed the performance of the four source term packages under different sea conditions including TCs. Their results agree with Kalourazi et al. (2021), concluding that the ST4 package performed best for wave simulation under relatively weak TC forcing, whilst ST6 had better performance under strong TC forcing.

Kaiser et al. (2022) conducted extensive comparisons of ST4 and ST6 for the South Atlantic and concluded that both source terms packages can produce good results when appropriately calibrated.

The studies above provide no clear guidance as to the preferred source term package for TC applications. Therefore, the ST4 and ST6 source term packages from the WW3 model were investigated here using the same eight North Atlantic hurricanes discussed above. Simulations were carried out for both, ST4 and ST6 source term packages, and results were compared against in-situ buoy measurements. The ST4 package used the T471 run calibrated for global ECMWF wind forcing conditions and the ST6 package used the standard CFSR calibration which runs with the default parameters such as CDFAC 1.0 for the wind drag coefficient (Zieger et al., 2015).

The source term packages produced similar results and errors and TC wind field parameters are probably a greater source of error than the choice of source term package. The one area where the packages diverged significantly was in the eye and weak wind side of the storm (considering values of H_s and f_p compared to buoys). This is illustrated in Fig. 5 for Hurricanes Ivan (Fig. 5a) and Ike (Fig. 5b). In both cases, H_s values from the ST6 source term package are smaller in magnitude than for ST4. It is likely that this is due to the stronger negative wind input source term in the ST6 formulation (Fig. 6a), where there is a negative growth rate under opposing winds (Donelan et al. (2006); Zieger et al. (2015)). There is limited in situ data to determine which of these results best models the actual situation for typical TC wave fields. The track of Hurricane Ike, however, passed directly over NDBC buoy 42001 and hence, it was possible to compare the recorded data with the source term packages (Fig. 5b). In this case, the ST4 simulation agrees better with the buoy data than ST6 in the eye of the storm.

Noting this limited buoy data, the identified differences between the source term packages, the performance of the ST4 package for the eight validation hurricanes and the longer application history with ST4, it was decided to use the ST4 physics package for the subsequent database generation. The input and dissipation ST4 parameterizations (Ardhuin et al., 2010) were applied using the nonlinear interaction module DIA (discrete interaction approximation, switch name NL1), higher-order and third-order propagation schemes (PR3 and UQ), wind linear interpolations for time and speed (WNT1 and WNX1), no bottom friction (BT0) and no depth-induced breaking (DB0).

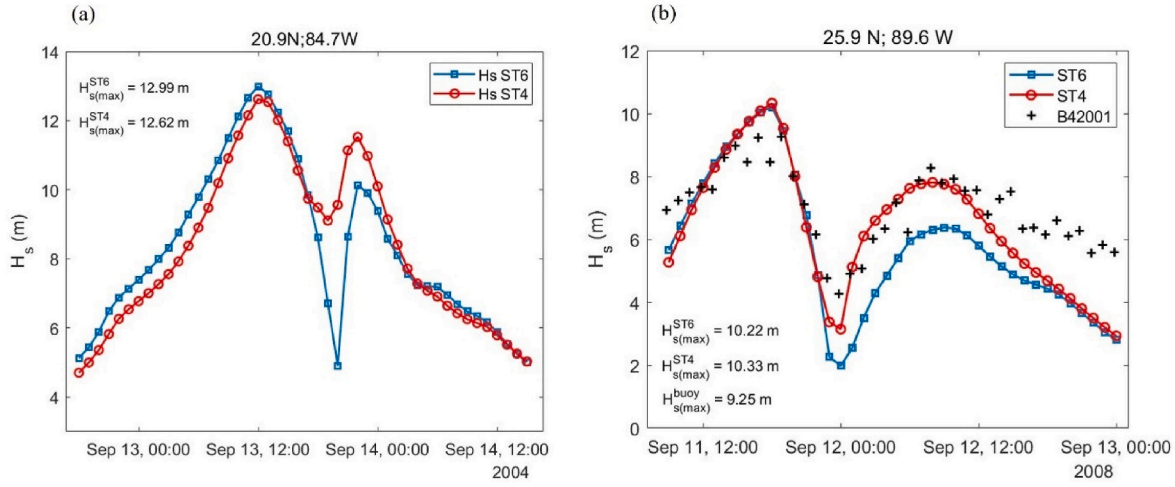

Fig. 5. Significant wave height (H_s) from WW3 results using ST4 (circle marker red line) and ST6 (square marker blue line) source terms packages. (a) H_s time series for location 20.9°N; 84.7°W where the storm center of Hurricane Ivan passed on 13 September 18:00 UTC and in (b) H_s time series at the position of NDBC buoy 42001, where the storm center of Hurricane Ike passed on 11 September 21:00 UTC.

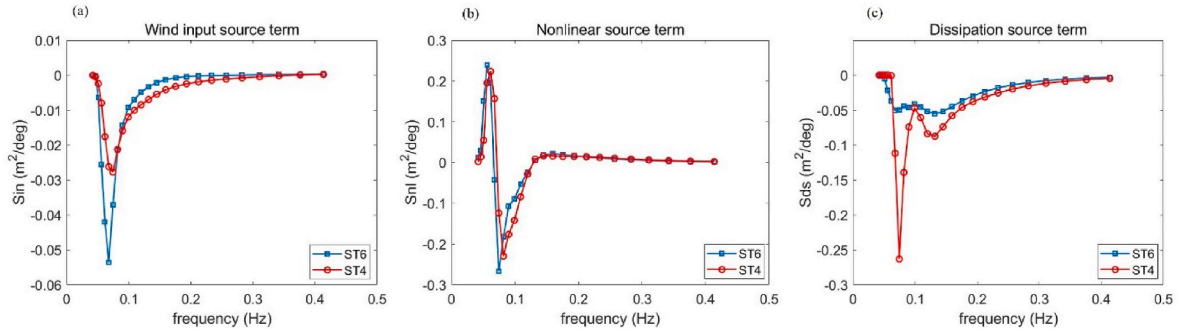

Fig. 6. Comparison between the source terms for ST4 (red) and ST6 (blue) packages. (a) S_{in} (wind input source term), (b) S_{nl} (Non-linear source term) and (c) S_{ds} (dissipation source term) for the Hurricane Ike on 11 September of 2008 at 21:00 UTC (eye of storm).

3.2. Moving grid implementation of WW3

The small spatial scale of TCs means that a WW3 implementation requires a high spatial and temporal resolution (Surgi et al., 1998; Chao et al., 2005; Chao and Tolman, 2010). In addition, as TCs can propagate thousands of kilometers over many days during their lifetime, the grid also needs to be of large spatial extent. To address these conflicts of scale, NOAA's National Center for Environmental Prediction (NCEP) has developed, multi-grid and two-way nesting capabilities in WW3, that include a version featuring a continuously moving spatial grid (Tolman and Alves, 2005). The moving grid feature allows the following of a TC wind field displacement using a limited high-resolution spatial domain, which significantly reduces computational cost, whilst maintaining the needed high resolution. The option to add a given continuous advection speed to the grid was implemented in WW3 model version 3.02 and is described in Tolman and Alves (2005). Other applications using the movable spatial grid can also be found in Alves et al. (2004) and Tamizi et al. (2021).

In the moving grid approach the movement of the storm, i.e., the velocity of forward movement (V_{fm}), is included in the advective terms of the energy balance equation (Tolman and Alves, 2005). The resulting model is set up for deep water on Cartesian grids without coastlines or land masses. The balance equation for this approach becomes:

$$\frac{\partial E(f,\theta)}{\partial t} + \left(C_g - V_{fm}\right) \cdot \nabla_x E(f,\theta) = S(f,\theta) \tag{4}$$

where f and θ are the spectral frequency and direction, respectively, E is the directional wave spectrum, C_g is the wave group velocity of the spectral component and ∇_x is the spatial gradient differential operator. S represents the contribution of sources and sinks in wind-wave evolution.

The motion of the grid has an influence on the Garden Sprinkler Effect (GSE), due to different retention times in the grid of spectral components with identical frequency but different propagation directions. Swells with longer retention time in the moving grid (waves ahead of the storm) tend to show a more pronounced GSE. Therefore, a modification to the GSE alleviation technique is necessary for this approach. To address this issue, Tolman and Alves (2005) introduced a tuning parameter (p) to the standard GSE alleviation method, smoothing the GSE asymmetry in the forward and backward faces of the wave height field. For $p = 0$, no correction is applied, whilst for $p = 1$ the averaging area is scaled linearly with the retention time of the spectral component in the moving grid.

3.2.1. Movable grid experiment

As the validation results for the historical U.S. hurricanes in Section 3.1 were obtained with a stationary grid (WW3 conventional fixed grid model), it is important to demonstrate that the moving grid version of WW3 produces approximately the same results as the stationary grid. To address this, a series of tests were undertaken with both stationary and moving grid versions of WW3, covering a range of TC parameters (Δp, V_{fm}, R_{max} and R_{34}).

Cartesian rectangular grids with a spatial resolution of 2 km were defined for both experimental setups. The spatial extent for the movable grid was set as 600 km in both east-west and north-south directions. The stationary grid used the same east-west extent (600 km), however in the north-south direction the spatial extent was 1500 km. The test cases used TCs that propagated towards the north and this extended stationary grid provided sufficient coverage for the storms to reach full development (e.g. 48 h for a translation speed of 7.5 m/s). In general, the time needed for both H_s and T_p to reach equilibrium was approximately 24 h in all tested cases.

Note that the spatial extent of the movable grid (600 km) used in these tests and subsequent runs was chosen to be large enough to encompass the major tropical cyclone forcing. For a typical value of $R_{max} = 30$ km, this provides a spatial extent of $\pm r/R_{max} = 10$. Young (2006) and Tamizi and Young (2020) show that for $r/R_{max} > 8$, the tropical cyclone wave field becomes very dependent on background winds and distant swells.

For the continuously moving grid runs, three switches were included in the WW3 run files. The MGP that activates the propagation correction scheme, the MGW that applies wind correction in the moving grid approach and the MGG that activates the GSE alleviation correction.

Tests were performed with the storm moving to the North with $V_{fm} =$ 2.5, 5.0 and 7.5 m/s and $\Delta p = 30$, 50 and 70 hPa (p_0 equivalent to 980, 960 and 940 hPa, respectively). Fixed values for R_{max} and R_{34} were chosen as 30 and 300 km, respectively. This represents a total of 9 validation runs.

As an example, Fig. 7 shows the spatial distribution of H_s and $T_p = 1/f_p$, for the case of $V_{fm} = 7.5$ m/s, $\Delta p = 50$ hPa, $R_{max} = 30$ km and $R_{34} = 300$ km. This case would be similar to a moderate to intense hurricane (category 2 to 3), with a central pressure is 960 hPa and maximum wind speed of 43 m/s. It is clear from Fig. 7, that there is no significant difference in H_s or T_p between stationary and moving grids. The maximum significant wave height (H_s^{max}) for the moving grid was 14.4 m, whilst for the stationary grid simulation this value was 14.1 m (2% difference). Fig. 7c and d also show quite similar T_p distributions. The value of T_p related to H_s^{max} for the moving grid simulation was 14.9 s ($f_p = 0.0672$ Hz), while for the stationary grid simulation the $T_p = 14.8$ s ($f_p = 0.0674$ Hz).

There is a slightly more pronounced GSE in the significant wave height field for the moving grid simulation for waves moving ahead of the storm (Fig. 7a) when compared to the fixed grid simulation. The default tuning value of $p = 0.5$ was applied for the simulation using the movable grid.

Across all simulation tests, the maximum difference in H_s^{max} was 2.36%, with the average across all cases being 1.75%. It was also noted that there was a small positive bias for all moving grid simulations. Based on these results, it is concluded that the moving grid simulations

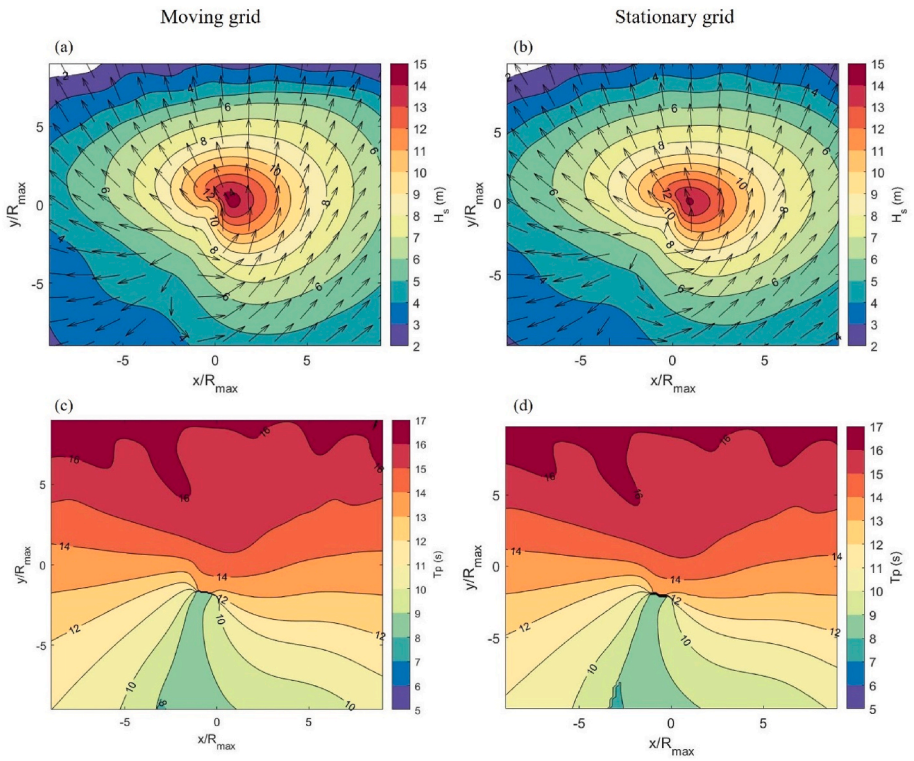

Fig. 7. Comparison between WW3 simulations with moving grid (left panels) and stationary grid (right panels). (a,b) Contour plots of significant wave height H_s (m) and vectors of the peak wave direction θ_p (not scaled). (c,d) Contour plots of peak wave period T_p (s). The spatial scale is normalized by R_{max} and TC parameters used were: $V_{fm} = 7.5$ m/s, $\Delta p = 50$ hPa, $R_{max} = 30$ km and $R_{34} = 300$ km. In both simulations the storm is propagating towards the North (up the page).

produce comparable results to the stationary grid setup, validated in Section 3.1, above.

3.3. Tropical cyclone synthetic database

The moving grid implementation of WW3 described above was subsequently used to run a large set of idealized TCs with a broad parameter space defined by: p_0, V_{fm}, R_{max} and R_{34}. To determine the appropriate parameter ranges for these values, data from the full global IBTrACS database were investigated.

Emanuel (2000) analyzed the statistical behavior of TC intensity from best track data for North Atlantic and Western North Pacific basins and found a potential maximum wind intensity of ~75 m/s. Kossin (2018) analyzing time series of annual mean translation speed based on IBTrACS data, finding an annual mean $V_{fm} \sim 8$ m/s for TCs over water. Chan and Chan (2015) and Mok et al. (2018) show a global mean of $R_{34} = 236$ km with 25th and 75th percentiles of 157 km and 290 km, respectively. Vickery and Wadhera (2008) analyzing the relationship between R_{max} and Δp for North Atlantic hurricanes, finding R_{max} varying between 15 and 50 km. Chavas and Knaff (2022) considered two North Atlantic hurricane datasets, finding 25th and 75th percentiles for R_{max} of 30 km and 60 km and for R_{34} of 100 km and 250 km, respectively.

For the present application, we considered data from the IBTrACS database for the North Atlantic and Western Pacific basins. Only storms for which the reported wind speed exceeded the threshold of 30 m/s were considered. Fig. 8 shows the joint distribution of the parameters V_{fm}, R_{max} and R_{34} for these basins.

Based on the results in Fig. 8, the following range of parameters were deemed reasonable to cover cases commonly encountered:

- $0 \leq V_{fm} \leq 15$ m/s, with an interval of 2.5 m/s;
- $R_{max} = 15$ km, 30 km and 60 km;
- $R_{34} = 200$ km, 300 km and 400 km;
- 10 hPa $\leq \Delta p \leq$ 150 hPa, with an interval of 20 hPa;

For all simulations the ambient atmospheric pressure was 1010 hPa and p_0 was calculated depending on the value of Δp. Values of V_{max} were not directly defined, but were calculated by the parametric wind field model based on the selected Δp and V_{fm}. To cover the full (four dimensional) parameter range described above involved approximately 400 WW3 moving grid simulations.

Based on a series of initial tests, it was determined that the moving grid simulations generally reached equilibrium within 1.5 days. To ensure this was the case, data were output after a simulation time of 2 days. This spin-up time agrees with typical regional wave and weather forecasts (e.g., Donelan et al., 2012; Ma et al., 2021). The default WW3 initial conditions were selected for all runs, defined via JONSWAP relations. In all simulations the moving grid moved to the North with the wind field asymmetric, with higher winds to the right (Northern Hemisphere) of the storm center. The model domain was 600 km × 600 km resolved with a spatial resolution of 2 km.

The computational discrete directional spectrum used in the model solution was defined with the model default increment factor of 1.1. The lowest spectral frequency was set at 0.05 Hz (minimum wave period of 20 s). Following a range of test cases, the frequency range was defined with 32 bands with the highest band of 0.96 Hz (1.04 s), defined by $f_n = 1.1 f_{n-1}$. A series of test runs were also performed with alternative spectral resolutions. These included using 44 bands to check the impact of extending the spectrum to higher frequencies, as well as a frequency increment of 1.07 and 50 frequency bands. Extending the spectrum in this manner had only insignificant impacts on the computed wave field. The number of direction bands was set at 36 (directional resolution of 10°), with the first direction set at 0.5°.

Fig. 9 presents an example of the results from this large range of model simulations. It shows values of the maximum significant wave height, H_s^{max} and the corresponding group velocity of these maximum waves, C_g^{max} as a function of V_{fm} and V_{max} for the case where $R_{max} = 30$ km and $R_{34} = 200$ km. The results show that H_s^{max} within the TC

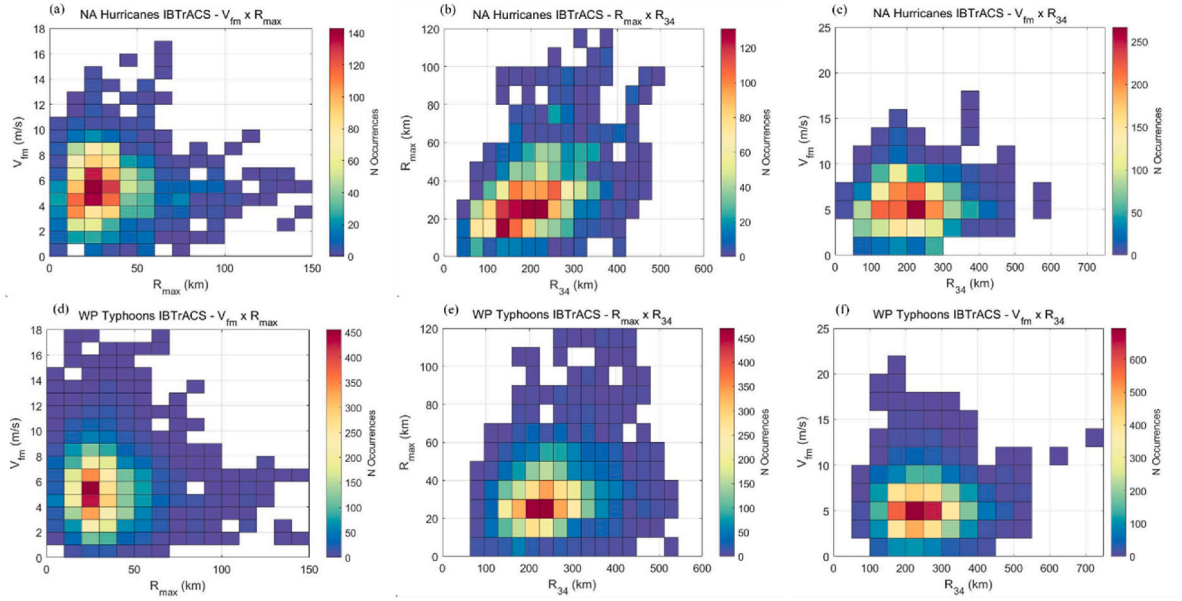

Fig. 8. The joint distribution of V_{fm}, $R_{\max}$ *and* R_{34} from IBTrACS dataset for (a to c): North Atlantic and (d to f): Western Pacific (d to f). Number of occurrences are shown as count values in the colour scale.

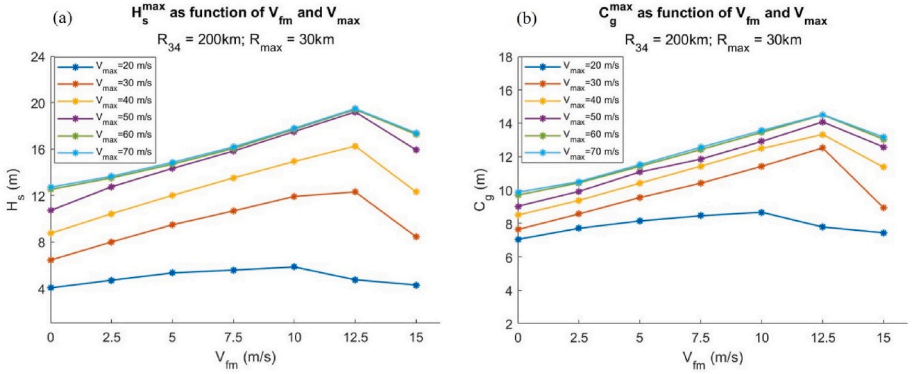

Fig. 9. (a) Maximum significant wave height, H_s^{max} and (b) associated maximum group velocity, C_g^{max} in a TC as a function of velocity of forward movement, V_{fm} and maximum wind velocity, V_{max}. Case shown for $R_{max} = 30$ km and $R_{34} = 200$ km.

increases as both V_{fm} and V_{max} increase. At values of $V_{fm} \approx 12.5$ m/s, a maximum is reached. At larger values of V_{fm} the storm appears to move too fast, and H_s^{max} begins to decrease (Fig. 9). The peak frequency (f_p) related to the values of H_s^{max} were used to calculate the resulting C_g^{max}. The results show that C_g^{max} also increases as a function of V_{fm} and V_{max} until reaching a peak in a similar pattern to H_s^{max} (Fig. 9b). Results for all the combinations of TC parameters show a similar pattern of behavior, consistent with the concept of an extended fetch within the TC (Shemdin (1977); King and Shemdin (1978); Young (1988); Young and Burchell (1996); Young and Vinoth (2013)). The extended fetch concept postulates that waves generated in the intense wind regions (right side of the storm in the North Hemisphere) can remain aligned with the wind for longer period of time and propagate forward with the storm. However, for storms moving faster than the wave group velocity, the peak waves in the spectrum are left behind the storm.

The present results provide the basis to expand the work of Young (1988), and investigate in detail this concept with a wave model using a contemporary representation of the nonlinear source terms, extending the preliminary results of Alves et al. (2004). The inclusion of the nonlinear terms in the model means that, compared to the results of Young (1988), there is a stronger transfer of energy to longer waves and, hence wave growth can be sustained for faster moving TCs than previously believed. This idea is also supported by Moon et al. (2003) and Zieger et al. (2021b). Moon et al. (2003) investigated the wavefield generated by TCs using the WW3 model and confirmed the central role of nonlinear wave-wave interactions. Zieger et al. (2021b) evaluated the parametric model of Young (1988) and its two updated versions (Young and Burchell, 1996; Young and Vinoth, 2013) and pointed out model limitations due to the omission of the non-linear interaction term in the estimation of wave field distributions. In particular, the limited transfer of energy to lower frequencies in these earlier forms of parametric model mean that values of H_s in such models seldom exceed approximately 10 m.

Young et al. (2020) showed that for Southern Ocean wave systems, nonlinear transfer was capable of a sustained energy transfer to waves propagating faster than the local wind. In the context of tropical cyclones, Tamizi et al. (2021) showed a similar situation with wave (swell) components propagating ahead of the TC still receiving significant energy transfer from the local wind-sea through nonlinear transfer. As shown above, this sustained transfer of energy from the wind-sea modifies the concept of the extended fetch in TCs. The extended fetch still exists, however, it is less likely that TCs will move so fast that they will effectively "outrun" the TC. Rather, as shown by the present results, and illustrated in Fig. 9, the continual feed of energy to the dominant waves through nonlinear transfer means that even for high values of V_{fm},

the effective fetch continues to increase, and the waves continue to receive energy from the TC. The energy transfer is not, however, directly from the local wind. Rather, the local wind transfers energy to the local wind-sea, which transfers it to the dominant waves through nonlinear transfer. As shown by Tamizi et al. (2021) this energy transfer can even shift energy to low-frequency components propagating at large angles to the local wind direction (exceeding 90°).

4. Parametric significant wave height model

As noted in Section 1, numerous observational studies (e.g. Young, 2006; Hu and Chen, 2011; Collins et al., 2018; Tamizi et al., 2020; Walsh et al., 2002) have shown that TC wave spectra are directionally skewed but their one-dimensional form (omnidirectional) is very similar to fetch-limited forms (e.g. Hasselmann et al., 1980; Donelan et al., 1985). Tamizi et al. (2021) have confirmed that this is a result of nonlinear wave-wave interactions playing a dominant role in shaping the spectra of waves generated within TCs. This explains the apparent success of parametric significant wave height models which represent the TC wave field in terms of an equivalent fetch and JONSWAP-style growth relationships (Young, 1988; Young and Burchell, 1996; Young and Vinoth, 2013). The present results provide a comprehensive database allowing the representation of this equivalent fetch.

As proposed by Young (1988), we adopt a modified form of the JONSWAP (Hasselmann et al., 1985) fetch-limited relationship to represent H_s^{max}.

$$\frac{gH_s^{max}}{V_{max}^2} = \alpha 0.0016 \left(\frac{gF}{V_{max}^2}\right)^{0.5} \tag{5}$$

where F is the equivalent fetch for a given TC. For each wave field in our database generated with WW3, (5) can be solved to determine F. The parameter α is a calibration term, which, was set to 1.0 in the validation runs and fetch calculation below. Based on these validation results, a value of $\alpha = 0.89$ is subsequently recommended (section 4.1).

Fig. 10 shows contour plots of the equivalent fetch (F) as a function of the TC parameters V_{fm}, V_{max}, R_{max} and R_{34}. The dependence of F on V_{fm} and V_{max} is similar to that previously identified by Young (1988), Young and Burchell (1996) and Young and Vinoth (2013). For a given V_{max}, F increases until it reaches a maximum, as shown in Fig. 9. This is the trapped fetch concept where the waves move forward with the TC translation speed. For a given V_{fm} a similar maximum is also reached as V_{max} increases. This does not, however, mean that H_s^{max} reaches a maximum and decreases at high values of V_{max}. Such a result would be counter intuitive (smaller waves at higher wind speed). Rather, as both F and V_{max} are parameters in (5), the combination of these parameters results in continued growth of H_s^{max} as V_{max} increases.

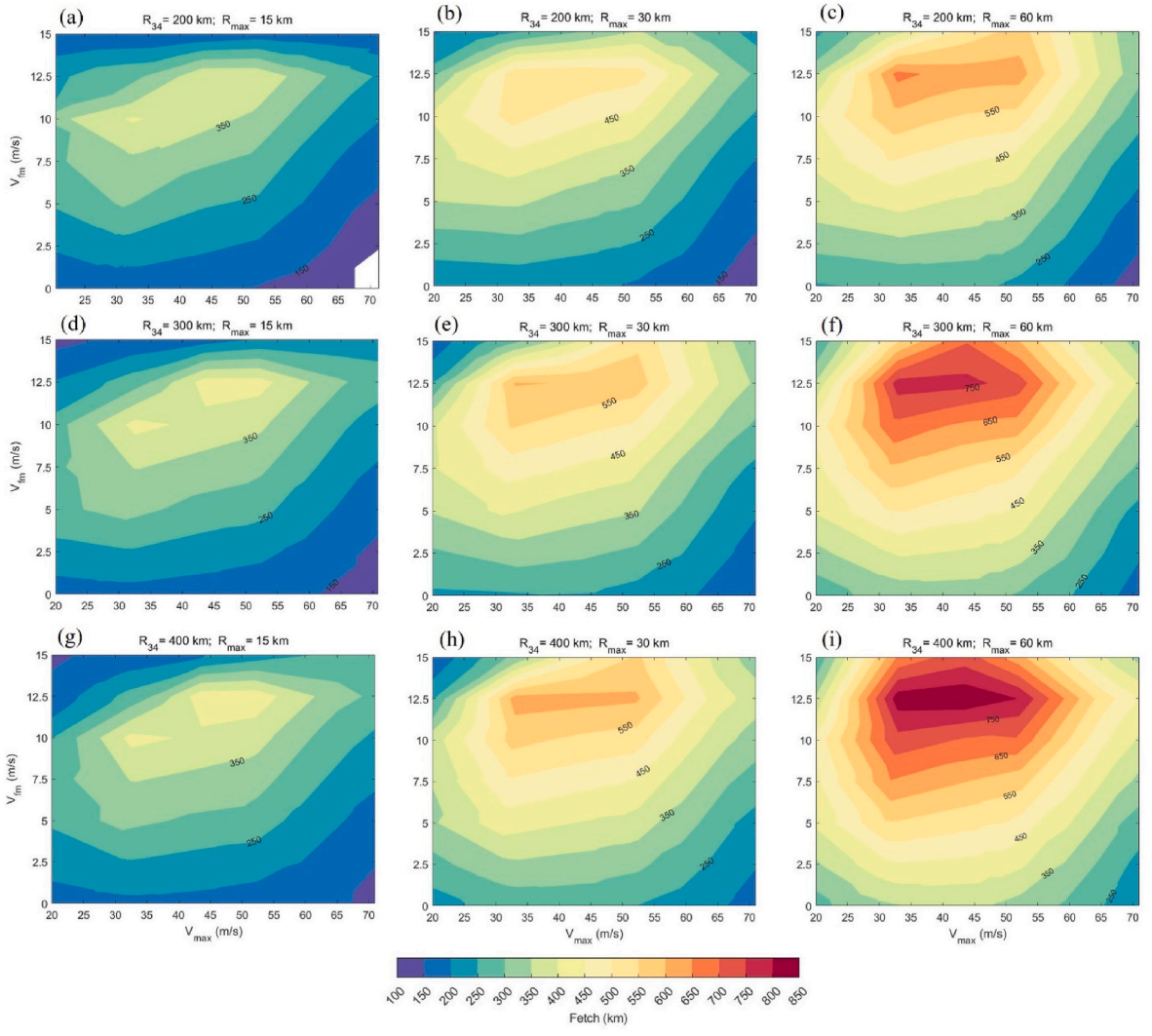

Fig. 10. Contour plot of the calculated equivalent fetch, F (km) as function of V_{fm} (m/s) and V_{max} (m/s). From left to right the vertical panels show $R_{max} =$ 15, 30 and 60 km. From top to bottom the horizontal panels show $R_{34} =$ 200, 300 and 400 km.

Fig. 10 also shows that F increases as both R_{max} and R_{34} increase. This is not surprising as the spatial scale of the TC increases with both parameters. This results in both more total energy in the storm and reduced curvature of the wind field (Alves et al., 2004). Both of these elements would be expected to increase F. The fact that F scales with R_{max} was previously identified by Young (1988).

Grouping the data by R_{max} and R_{34} and normalizing by $R_{max} = 30$ km and $R_{34} = 300$ km proved useful to quantify how the spatial scaling varies with each parameter. Curve fitting the results yields spatial scaling parameters as follows in equations (6) and (7).

$$\lambda = 0.85 \log_{10}\frac{R_{max}}{30 \times 10^3} + 1 \tag{6}$$

$$\gamma = 0.65 \log_{10}\frac{R_{34}}{300 \times 10^3} + 1 \tag{7}$$

In (6) and (7) R_{max} and R_{34} both have units of meters.

Noting these scaling relationships, the equivalent fetch, F was approximated by the third order polynomial as follows in equation (8).

$$\frac{F}{\lambda\gamma} = \left[aV_{max}^3 + bV_{max}^2 + cV_{fm}^2 + dV_{max}^2 V_{fm} + eV_{max}V_{fm}^2 + fV_{max}V_{fm} + gV_{max} + hV_{fm} + i\right]\exp\left(CV_{fm}\right) \tag{8}$$

where $C = 0.1$ and the terms a to i were determined from a least-squares curve fit and are shown in Table 2. Both V_{fm} and V_{max} have units of m/s.

For given values of V_{fm}, V_{max}, R_{max} and R_{34}, (6) to (8) define the equivalent fetch, F. This fetch can be used with the modified JONSWAP relationship (5) to determine H_s^{max}. The full spatial distribution of H_s can then be determined in non-dimensional form H_s/H_s^{max}. Values of H_s at any location can be determined by interpolating amongst the spatial distributions in the database generated by the WW3 model. This involves four-dimensional interpolation for the given values of V_{fm}, V_{max}, R_{max} and R_{34}. Typical spatial distributions from the database are shown in Fig. 11. In this example a TC with $V_{fm} = 5$ m/s and $V_{max} = 50$ m/s is shown. The resulting values of H_s/H_s^{max} are shown for $R_{max} = 15$ km (Fig. 11 a,d,g), 30 km (Fig. 11 b,e,h) and 60 km (Fig. 11 c,f,i), and for $R_{34} = 200$ km (Fig. 11 a,b,c), 300 km (Fig. 11 d,e,f) and 400 km (Fig. 11 g,h,i). Spatial distances are presented in nondimensional form in terms of r/R_{max} , where r is the radial distance from the storm center (in km) and R_{max} is the radius to maximum winds, here 30 km.

4.1. Validation of the parametric tropical cyclone wave height model

To evaluate the performance of the full TC wave height parametric model (PModel), predictions of H_s were validated against data from 25 buoys deployed during the passage of 17 North American hurricanes. The data includes the same eight historical hurricanes used for validation of both the wind field model and the WW3 wave model. In addition, a further nine hurricanes were included to extend the dataset (Edouard, Floyd, Lili, Wilma, Dean, Sandy, Joaquin, Maria, and Sam). The values of the maximum significant wave height predicted by the parametric model, H_s^{PModel} are shown in Table 1 (column 7, presented in section 3.1). The IBTrACS best track database was used to define the track and TC wind field parameters as previously described in section 3.1 (IBTrACS).

The comparisons between the parametric model significant wave height (H_s^{PModel}) and the significant wave height measured by the buoys (H_s^{buoy}) in Table 1 show that, in the majority of cases the parametric model is positively biased (larger H_s than buoys). Such a positive bias is not unexpected. The parametric model was developed from a synthetic database of fully-developed storm conditions. That is, the synthetic dataset was for storms with constant wind field parameters propagating in a straight line in deep water far from land. Application of the parametric model to practical TC conditions means that when a storm changes direction or intensifies the parametric model will instantaneously transition to a new fully developed state for the new propagation direction or wind field parameters. Similarly, finite depth or land masses (even distant from the TC) will also result in a positive bias. The only case where the parametric model would be expected to underestimate the wave height field would be for a decaying storm. Decaying storms generally occur after landfall and hence will seldom appear in data such as Table 1 of maximum recorded significant wave height.

There are three cases in Table 1 with quite large bias, all in finite depth water. Buoy 42035 (16 m water depth) which recorded during Hurricane Ike, buoy 41036 (30 m water depth) which recorded during Hurricane Irene, and buoy 41009 (40 m water depth) which recorded during Hurricane Matthew, show values of bias of 54%, 39%, and 43% respectively. In these cases, the large bias seems to be a result of decreased significant wave height due to the finite water depth. Excluding these cases, the overall bias of the parametric model is approximately 11% (absolute bias of 1 m) (Table 1). Fig. 12 shows a scatter plot comparing the maximum recorded significant wave height and the predictions from the parametric model. Analyzing these results the calibration factor α in equation (5) was set to 0.89.

The analysis above and shown in Fig. 12 concentrates on the maximum H_s predicted by the parametric model, an important metric for most applications. However, we also investigated comparisons of values of H_s when the storms were further from the buoys. Data for each of the validation cases were considered over the period of 12 h before and 6 h after the closest approach of the hurricanes to each buoy. The 6 h period is to avoid landfalling cases. Quantile-quantile (QQ) plots were used to compare the buoy and parametric values of H_s. In contrast to the above case for the maximum values, these results showed the parametric model slightly underestimated the buoys. The reason for this is not clear. It is possible that the spatial extent of the hurricane vortex wind field is smaller than in reality, either due to limitations of the vortex model or the IBTrACS parameters used. It is also possible that at lower values of H_s, when the hurricane is distant from the buoy, background swell becomes more important. As the parametric model does not model this swell, one would expect the model to underestimate.

The above results are for the maximum values of H_s during the passage of TCs. To provide an indication of parametric model performance in terms of the spatial distribution of significant wave height, two well documented storms are considered below, one from the Gulf of Mexico (Hurricane Ivan) and other from the North Atlantic (Hurricane Irene).

4.1.1. Case 1: Hurricane Ivan

As mentioned in section 3.1.1, Hurricane Ivan crossed the North Atlantic and Gulf of Mexico in September 2004 and reached category 5. The storm track from 12:00 UTC 14 September to 21:00 UTC 15 September is shown in Fig. 13a. Values of H_s generated by Ivan were sampled by the radar altimeter carried by the ERS-2 satellite, when the storm was in the Gulf of Mexico. The ERS-2 track through the storm occurred between 04:04 and 04:06 UTC on September 15. The ground track of the altimeter is shown superimposed on the significant wave heigh field predicted by the parametric model in Fig. 13a. A comparison

Table 2
Coefficients for equation (8).

a	b	c	d	e	f	g	h	i
5.40×10^{-1}	1.69×10^{2}	1.44×10^{3}	3.99×10^{-1}	1.43×10^{1}	4.30×10^{2}	9.60×10^{3}	4.47×10^{3}	1.00×10^{5}

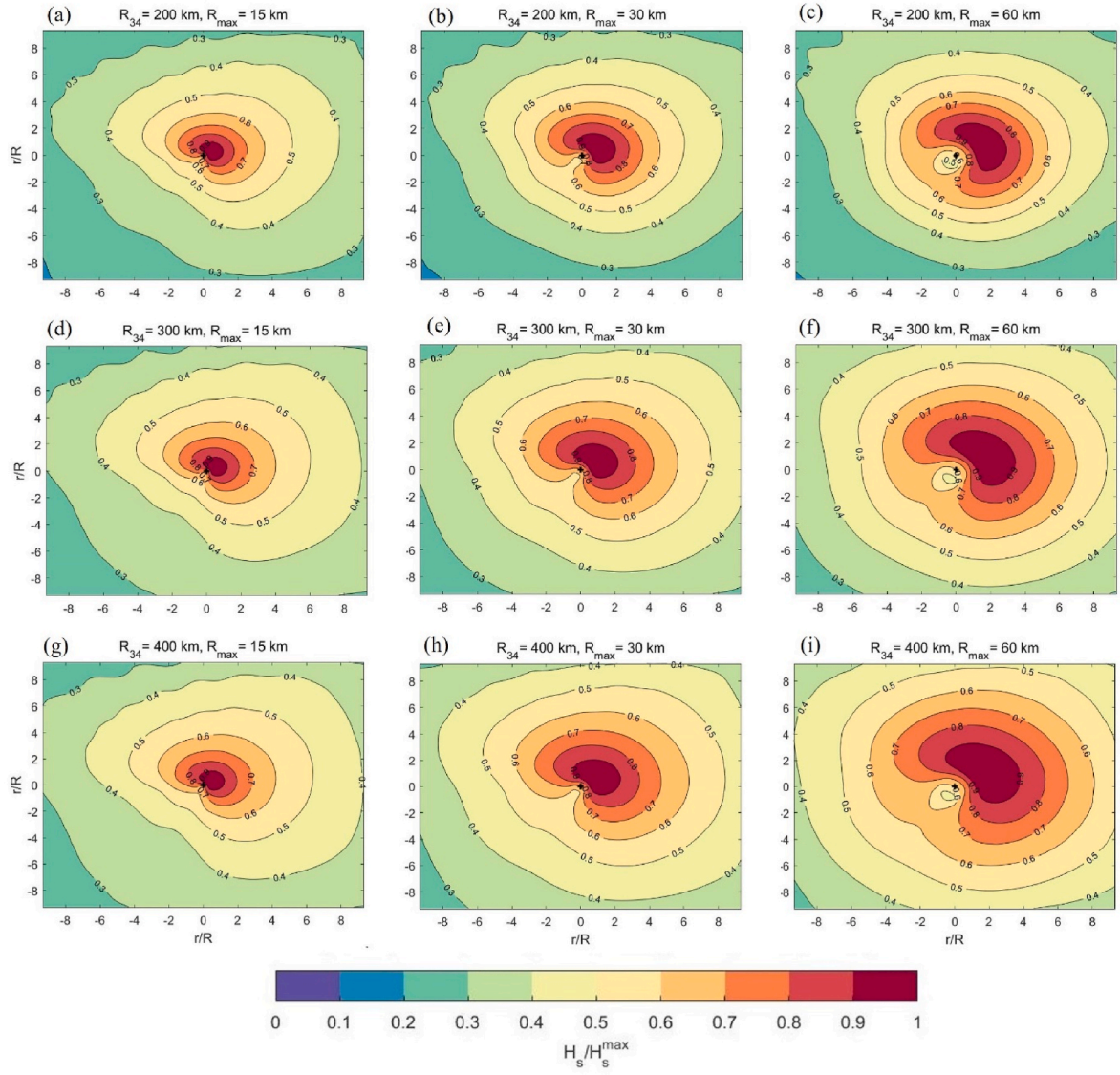

Fig. 11. Contour plot of the spatial distribution of H_s/H_s^{max} for a tropical cyclone with $V_{fm} = 5$ m/s and $V_{max} = 50$ m/s. From left to right vertical panels show results for $R_{max} = 15$ km (a,d,g), 30 km (b,e,h) and 60 km (c,f,i), and from top to bottom horizonal panels show results for $R_{34} = 200$ km (a,b,c), 300 km (d,e,f) and 400 km (g,h,i).

between values of H_s recorded by the altimeter (Ribal and Young, 2020) along the ground track and predicted by the parametric model are shown in Fig. 13b. The value of α in (5) was set at 1.0 (uncalibrated) for the following comparisons.

At the time of the altimeter overpass, the IBTrACS storm parameters used were $V_{\max} = 62$ m/s, $V_{fm} = 5$ m/s and $R_{34} = 345$ km. For this storm, there is no information for $R_{\max}$ provided by the IBTrACS dataset. Therefore, a value of 30 km, representative of TCs in the region (Fig. 8) was adopted.

Fig. 13 (b) shows that the parametric model can capture the spatial distribution of H_s measured by the altimeter with an underestimation up to 2 m ahead of the storm center (25.3° in latitude) and with an overprediction of approximately 1 m near the TC center. This result is consistent with the previous observations that the parametric model is biased high by approximately 10%–12%. A comparison such as that in Fig. 13 is also dependent on the accuracy of the storm track and parameters contained within the IBTrACS database.

NDBC buoy 42003 was located to the right (intense wind/wave side) of the storm track (Fig. 13a) and recorded 3-hourly H_s time series during the passage of the storm. This observed H_s data were compared with H_s calculated from the parametric model using the same IBTrACS wind field data (Fig. 14). The nearest point of approach between the storm and the buoy occurred at 06:00 UTC on September 15. The time series comparison shows that the parametric model predicts the general distribution of H_s, however, the model overestimates the maximum significant wave height by approximately 1 m (10%) when the storm passes nearest to the buoy. It also appears that the model peaks later than the buoy, suggesting that the either the track of IBTrACS or the wind field may not be optimal.

4.1.2. Case 2: Hurricane Irene

Hurricane Irene crossed the North Atlantic in late August 2011 and reached a Saffir–Simpson hurricane intensity scale (SSHS) of category 3. Values of H_s within Irene were sampled by the Jason-2 altimeter between 07:51 and 07:53 UTC on August 26. NDBC buoy 41010 was located to the left side (low wind/wave side) of the storm track (Fig. 15a). The IBTrACS parameters at the time of the altimeter pass were $V_{\max} = 46$ m/s, $V_{fm} = 6$ m/s, $R_{34} = 350$ km and $R_{\max} = 46$ km.

Fig. 15 (b) shows that the parametric model reproduces the peak values of H_s measured by the altimeter extremely well, as well as the

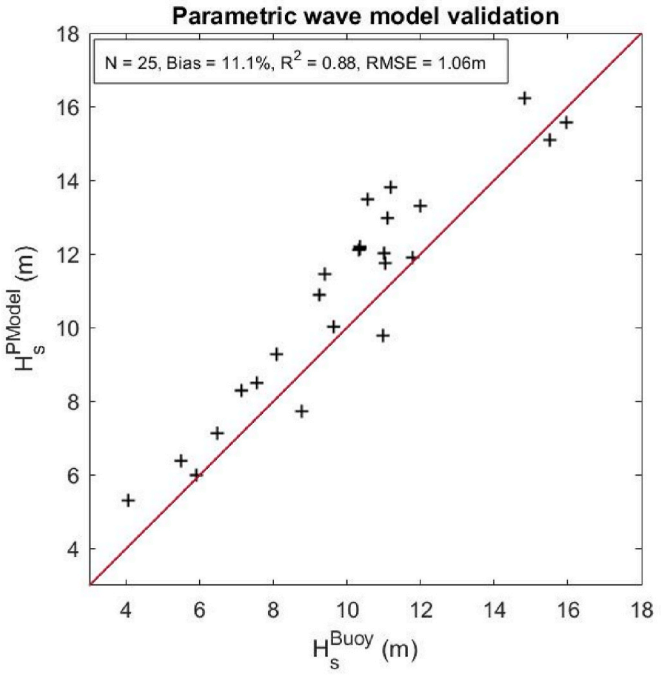

Fig. 12. Comparison of maximum significative wave height predicted by the parametric model (H_s^{Pmodel}) against maximum significant wave height recorded by NDBC buoys (H_s^{buoy}) during the passage of the hurricanes shown in Table 1. The skill metrics are shown in the box in the graphic and include bias, adjusted R-squared (R^2) and root-mean-square error (*RMSE*), *N* is the number of observations.

values ahead of the storm. For the region south of the hurricane center, the parametric model shows a significant over estimation in H_s. However, in this region, the altimeter track is through the Bahamas Islands, which explains the significant decrease in altimeter H_s and the over estimation by the parametric model (i.e. the parametric model cannot model the impacts of land).

NDBC buoy 41010 recorded 3-hourly values of H_s between 18:00 UTC 25 August and 18:00 UTC 26 August. The values of H_s measured by the buoy and predicted by the parametric model are shown in Fig. 16. The nearest point of approach between the storm and the buoy occurred at 06:00 UTC on August 26. The parametric model performs well in estimating the peak H_s, overestimating by 0.4 m (5%). Generally, however, the parametric model is biased high by approximately 1m (10%), consistent with the previous results when $\alpha = 1.0$.

4.2. Limitations and calibration of significant wave height TC parametric model

The validation results above show that the parametric TC model consistently overestimates values of H_s by approximately 11%. Such a positive bias is to be expected, as the model assumes the TC wave field can be approximated by a series of fully-developed simulations from WW3. In contrast, the full WW3 model shows almost no bias (Table 1). As a result, we conclude that a value of $\alpha = 0.89$ in (5) will yield appropriate values for most practical cases.

The validation results highlight a number of limitations of the model. As the parametric model assumes a fully developed storm, it will overestimate in cases where there is significant curvature or changes in the direction of the TC. An overestimation in H_s can also be expected in cases where there is a rapid intensification of the TC. For most practical cases, however, the calibration factor recommended above will approximate the conditions reasonably well. The parametric model is also for deep water and is not intended for finite depth applications. Similarly, it is also expected that the model will overestimate significant wave height in the proximity of islands or in enclosed basins (e.g. Gulf of Mexico).

Although the model is a parametric approximation of the TC wave field, it does capture our understanding of the physics of wave generation in such systems. It includes a representation of the role both the velocity of forward movement and the maximum wind velocity in the storm play in defining an extended fetch. In addition, the JONSWAP-style scaling used holds in such cases due to the dominant role played

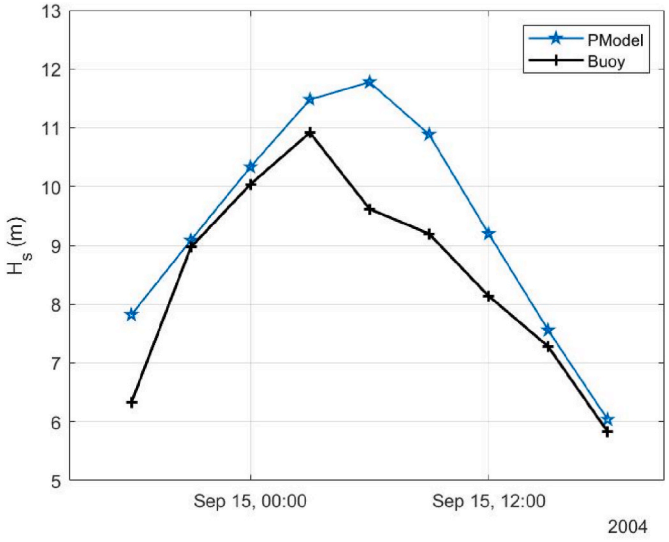

Fig. 14. Comparison between the measured H_s data from NDBC buoy 42003 and H_s simulated by the parametric model for Hurricane Ivan ($\alpha = 1.0$).

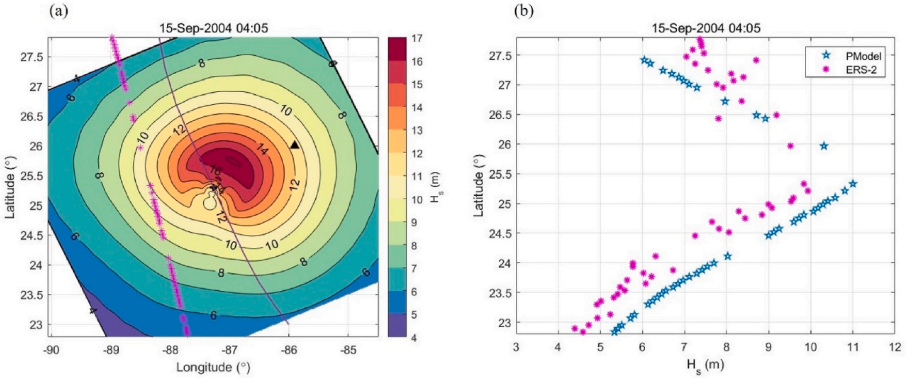

Fig. 13. On the left panel (a) significant wave height H_s (m) distribution determined from the parametric TC wave model for Hurricane Ivan ($\alpha = 1.0$). The asterisk (*) symbols in magenta show the ERS-2 altimeter track. The fine solid line SE-NW is the storm track, and the black triangle is the location of the NDBC buoy 42003. On the right panel (b) comparison between measured H_s data from the altimeter (magenta asterisk) and predicted H_s from the parametric model (cyan star) along the satellite track.

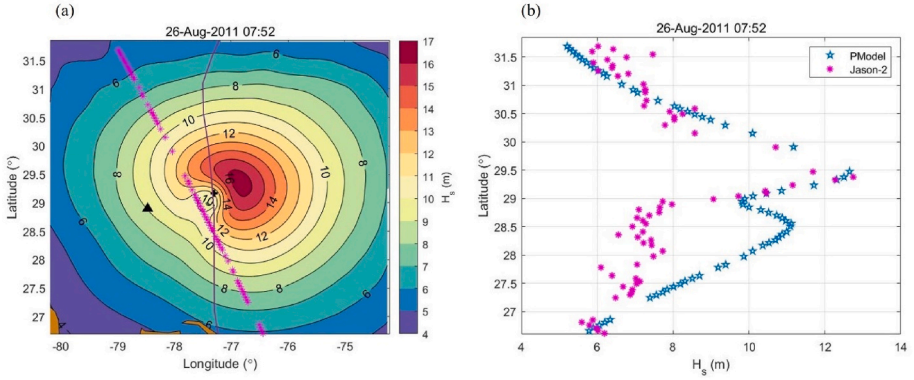

Fig. 15. (a) Significant wave height H_s (m) distribution predicted by the parametric model for Hurricane Irene ($\alpha = 1.0$). The asterisk symbols (*) in magenta show the Jason-2 altimeter track, the fine solid line orientated N–S is the storm track, and the black triangle is the location of the NDBC buoy 41010. (b) Comparison between measured H_s data from the altimeter (magenta asterisk) and predicted H_s from the parametric model (cyan star) along satellite track.

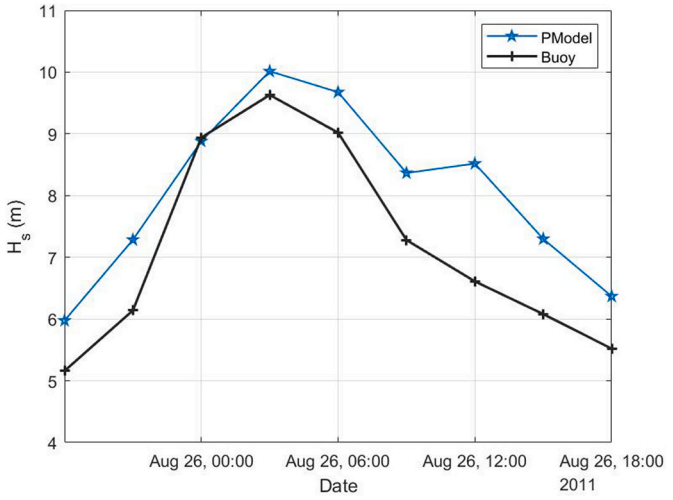

Fig. 16. Comparison between the measured H_s data from NDBC buoy 41010 and H_s predicted by the parametric for Hurricane Irene ($\alpha = 1.0$).

by nonlinear interactions. The use of a third-generation wave model to generate the synthetic database, upon which the model is based, approximates these processes. The model is also forced by an updated vortex wind model based on observed wind field asymmetry and inflow angle. Despite these advances, the model is an approximation to the TC wave field and has a level of sophistication consistent with the use of wind fields defined by best-track parameter approximations. For applications that do not require large numbers of realizations of the TC wave field, we recommend the use of a full spectral wave model.

5. Conclusions

The parametric TC model for significant wave height developed in this study updates previous approaches using the state-of-the-art third-generation spectral WAVEWATCH III model (WW3) to generate a synthetic database. In addition, quality is added to the resulting database by employing an updated wind vortex model based on observed wind field asymmetry and inflow angles, used to force WW3. Both the vortex wind field model and the WW3 model are validated against NDBC buoy data. The parametric significant wave height model confirms our understanding that wave generation within tropical cyclones is strongly determined by an extended fetch, which is a function of both the storm's velocity of forward movement and maximum wind speed. The JONSWAP-style scaling used to estimate the maximum significant wave height from this extended fetch is believed to hold in such cases due to the dominant role played by nonlinear wave-wave interactions in defining the wave spectrum and hence the significant wave height. As such, the parametric model is based on our present understanding of the physics of TC wind-wave generation and is supported by significant observational evidence.

The parametric model is developed using a comprehensive database of almost 400 simulations made with the WW3 model covering ranges of values for four parameters defining the TC wind/wave field (V_{fm}, V_{max}, R_{max} and R_{34}). Equations (6)–(8) define an equivalent fetch based on these parameters. This extended fetch can then be used in Equation (5) to define the maximum significant wave height within the storm. Determining the significant wave height at other locations within the TC wave fields requires interpolation within the field data from the four-parameter synthetic wave field WW3 database.

The final performance of the parametric model has been validated and calibrated against an extensive database of both buoy and altimeter data. The model is recommended for applications where computation efficiency is required where a large number of TC simulations are necessary (e.g. climatology and extreme value estimates). The model and the WW3 database can also be used to estimate peak wave frequency, mean wave direction and the detailed spectral form. Such extensions are planned for future work.

In comparison to earlier parametric models of this type (Young, 1988; Young and Burchell, 1996; Young and Vinoth, 2013), the present model has a sounder theoretical basis, as it is developed from data generated by a spectral model with a more sophisticated representation of the important nonlinear terms. As such, the present model would be expected to more reliably reproduce measured TC wave fields. The physical basis of the present model, as represented by the concept of the extended fetch, and the WW3 model used to develop the synthetic database is a significant advance over previous such models. It should be pointed out, however, that the DIA is still an approximation to the nonlinear source term, which represents a limitation. The resulting model has, however, been extensively validated against buoy and satellite data under a wide range of TC conditions, showing good results.

Application of model and code availability

Application of the model involves the following steps:

- Given V_{max} (or Δp), V_{fm}, R_{34} and R_{max}, Equation (8) provides the equivalent fetch, F.
- Equation (5) then provides $H_s^{\max}$.
- To obtain the spatial distribution of the wave field, values of $H_s/H_s^{\max}$ can be determined by 4-dimensional interpolation between values of 378 spatial distributions upon which the model is based. These spatial distributions and sample code to apply the parametric model

are available on Figshare at https://figshare.com/s/de3a1ceab6d165d29411

CRediT authorship contribution statement

Guisela Grossmann-Matheson: Conceptualization, Data curation, Formal analysis, Investigation, Methodology, Software, Validation, Visualization, Writing – original draft, Writing – review & editing. **Ian R. Young:** Conceptualization, Data curation, Formal analysis, Funding acquisition, Investigation, Methodology, Project administration, Resources, Supervision, Validation, Writing – original draft, Writing – review & editing. **Jose-Henrique Alves:** Investigation, Methodology, Resources, Validation, Supervision, Writing – review & editing. **Alberto Meucci:** Investigation, Methodology, Software, Supervision, Validation, Writing – review & editing.

Declaration of competing interest

The authors declare no competing interests.

Data availability

The data have been placed on a public repository. The link is given in the paper.

Acknowledgements

This work was financially supported by the University of Melbourne through a PhD scholarship. Computational resources for the extensive range of simulations used to construct the WW3 database were provided by NOAA Oceanic and Atmospheric Research (OAR) Weather Program Office (OAR) and are gratefully acknowledged.

Appendix

A) Example of results of the comparison of the parametric wind vortex model (updated Holland Model with IBTrACS parameters) and H*Wind post storm wind fields.

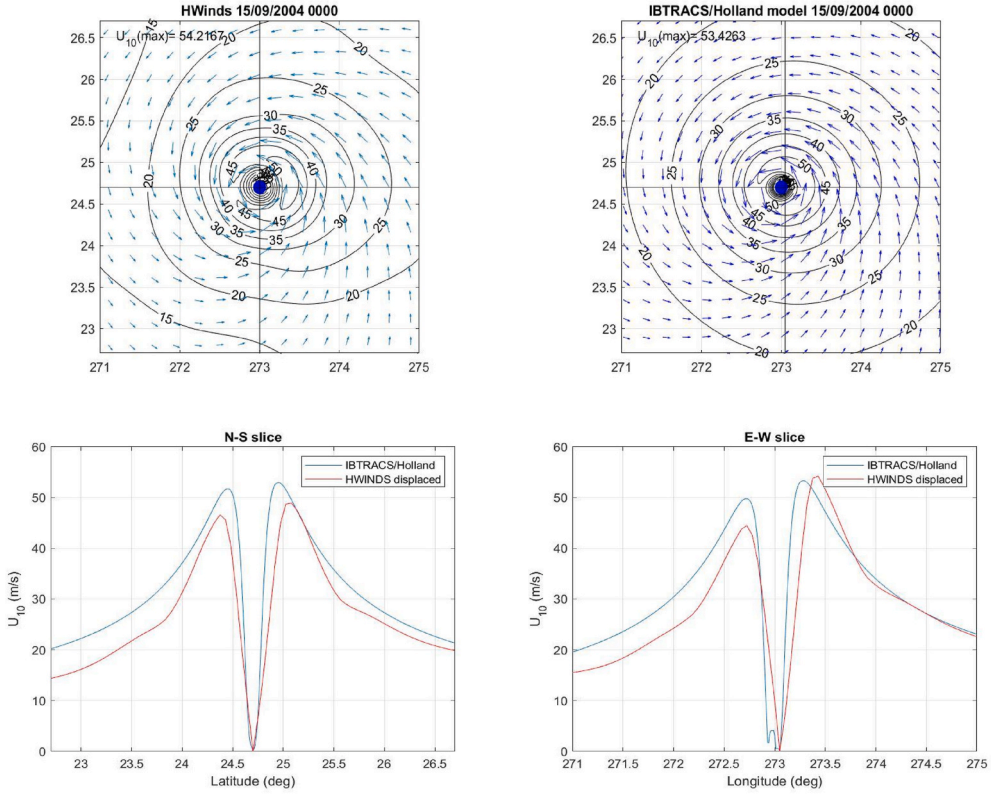

Fig. A1. Comparison between wind fields from the parametric wind vortex model and H*Wind reanalysis for Hurricane Ivan at 00:00 UTC Sep 15, 2004.

Table A1
Comparison of maximum wind velocity (U_{10}^{max}) between H*Wind reanalysis data and parametric wind vortex model (Holland/IBTrACS) for the eight selected hurricanes.

Hurricane	Date	U_{10}^{max} (m/s)		Bias (m/s) U_{10}^{PWind} - U_{10}^{HWind}
		H*Wind	Vortex Wind model	
Ivan	15/9/2004 00:00	54.2	53.4	−0.8
	15/9/2004 06:00	52.6	50.9	−1.7
	15/9/2004 18:00	49.3	49	−0.3

(*continued on next page*)

Table A1 (*continued*)

Hurricane	Date	U_{10}^{max} (m/s)		Bias (m/s) U_{10}^{PWind} - U_{10}^{HWind}
		H*Wind	Vortex Wind model	
Katrina	28/8/2005 00:00	42.9	46.9	4
	28/8/2005 18:00	62.3	60.9	−1.4
	29/8/2005 00:00	56.1	60.7	4.6
Rita	21/9/2005 01:30	37.7	35.9	−1.8
	22/9/2005 07:30	60.6	63.5	2.9
	23/9/2005 07:30	49.7	54.6	4.9
Gustav	31/8/2008 10:30	44.8	40	−4.8
	31/8/2008 16:30	38.9	40	1.1
	1/9/2008 1:30	43.6	43	−0.6
Ike	12/9/2008 1:30	38	42.3	4.3
	12/9/2008 13:30	42.2	42.1	−0.1
	12/9/2008 22:30	41.3	42.9	1.6
Earl	2/9/2010 7:30	53.4	53.2	−0.2
	2/9/2010 10:30	50.2	50.6	0.4
	3/9/2010 1:30	41.8	44.1	2.3
Irene	25/8/2011 01:30	42.1	43.9	1.8
	25/8/2011 13:30	40.3	44.5	4.2
	26/8/2011 13:30	42.7	44.9	2.2
Matthew	3/10/2016 0:00	48.3	48	−0.3
	6/10/2016 12:00	52.6	49.3	−3.3
	7/10/2016 0:00	49.5	49.6	0.1

References

Abdolali, A., van der Westhuysen, A., Ma, Z., Mehra, A., Roland, A., Moghimi, S., 2021. Evaluating the accuracy and uncertainty of atmospheric and wave model hindcasts during severe events using model ensembles. Ocean Dynam. 71 (2), 217–235. https://doi.org/10.1007/s10236-020-01426-9.

Abdolali, A., Roland, A., van der Westhuysen, A., Meixner, J., Chawla, A., Hesser, T.J., Smith, J.M., Sikiric, M.D., 2020. Large-scale hurricane modeling using domain decomposition parallelization and implicit scheme implemented in wavewatch III wave model. Coast Eng. 157, 103656 https://doi.org/10.1016/j.coastaleng.2020.103656.

Alves, J.H.G.M., Tolman, H.L., Chao, Y.Y., 2004. Hurricane-generated wind-wave research at NOAA/NCEP. In: Preprints, Eighth Int. Workshop on Wave Hindcasting and Forecasting. U.S. WMO/IOC/JCOMM, Hawaii, p. 13. G3. http://www.wavehindcasting.org/8thWaves/Papers/G3.pdf.

Alves, J.G.M., Stripling, S., Chawla, A., Tolman, H., van der Westhuysen, A., 2015. Operational wave guidance at the U.S. National weather Service during tropical/post–tropical storm Sandy, October 2012. Mon. Weather Rev. 143, 1687–1702. https://doi.org/10.1175/MWR-D-14-00143.1.

Amante, C., Eakins, B.W., 2009. ETOPO1 Global Relief Model Converted to PanMap Layer Format. NOAA-National Geophysical Data Center. https://doi.org/10.1594/PANGAEA.769615. PANGAEA.

Ardhuin, F., Chapron, B., Collard, F., 2009. Observation of swell dissipation across oceans. Geophys. Res. Lett. 36 (6), L06607 https://doi.org/10.1029/2008GL037030.

Ardhuin, F., Rogers, E., Babanin, A.V., Filipot, J.F., Magne, R., Roland, A., VanderWesthuysen, A., Queffeulou, P., Lefevre, J.M., Aouf, L., Collard, F., 2010. Semi empirical dissipation source functions for ocean waves. PartI: definition, calibration, and validation. J. Phys. Oceanogr. 40 (9), 1917–1941. https://doi.org/10.1175/2010JPO4324.1.

Babanin, A.V., 2011. Breaking and Dissipation of Ocean Surface Waves. Cambridge University Press.

Babanin, A.V., Young, I.R., 2005. Two-phase behaviour of the spectral dissipation of wind waves, 3-7 July, 2005, Madrid, Spain. In: Edge, B., Santas, J.C. (Eds.), Proc. Ocean Waves Measurement and Analysis, Fifth Int. Symp. WAVES2005, Sponsors CEDEX (Spain) and CORPI of ASCI (USA). paper no.51, 11p.

Babanin, A., Manasseh, R., Young, I., Schultz, E., 2007. Spectral dissipation term for wave forecast models, experimental study. In: Proc. 10 th Int. Workshop on Wave Hindcasting and Forecasting and Coastal Hazards Symp. US Army Engineer Research and Development Center, Oahu, HI, 19p.

Banner, M.L., Young, I.R., 1994. Modeling spectral dissipation in the evolution of wind waves - Part 1. Assessment of existing model performance. J. Phys. Oceanogr. 24, 1550–1671.

Beyramzadeh, M., Siadatmousavi, S.M., 2022. Skill assessment of different quadruplet wave-wave interaction formulations in the WAVEWATCH-III model with application to the Gulf of Mexico. Appl. Ocean Res. 127, 103316 https://doi.org/10.1016/j.apor.2022.103316. ISSN 0141-1187.

Bi, F., Song, J., Wu, K., Xu, Y., 2015. Evaluation of the simulation capability of the WavewatchIII model for Pacific Ocean wave. Acta Oceanol. Sin. 34 (9), 43–57. https://doi.org/10.1007/s13131-015-0737-1.

Bidlot, J.-R., 2012. Present status of wave forecasting at ECMWF. Proc. ECMWF Workshop Ocean Waves 25–27. June 2012.

Bidlot, J., Janssen, P., Abdalla, S., Hersbach, H., 2007. A Revised Formulation of Ocean Wave Dissipation and its Model Impact ECMWF. ECMWF Technical Memoranda.

Biswas, M.K., Bernardet, L., Abarca, S., Ginis, I., Grell, E., Kalina, E., et al., 2018. Hurricane Weather Research and Forecasting (HWRF) Model: 2017 Scientific Documentation (No. NCAR/TN-544+STR. https://doi.org/10.5065/D6MK6BPR.

Black, P.G., Coauthors, 2007. Air–sea exchange in hurricanes: synthesis of observations from the coupled boundary layer air–sea transfer experiment. Bull. Amer. Meteor. Soc 88, 357–374. https://doi.org/10.1175/BAMS-88-3-357.

Bowyer, P.J., MacAfee, A.W., 2005. The theory of trapped-fetch waves with tropical cyclones—an operational perspective. Weather Forecast. 20, 229–244. https://doi.org/10.1175/WAF849.1.

Campos, R.M., Gramcianinov, C.B., de Camargo, R., da Silva Dias, P.D., 2022. Assessment and calibration of ERA5 severe winds in the Atlantic Ocean using satellite data. Rem. Sens. 14 (19), 4918. https://doi.org/10.3390/rs14194918.

Cardone, V.J., Jensen, R.E., Resio, D.T., Swail, V.R., Cox, A.T., 1996. Evaluation of contemporary wave models in rare extreme events: the “Halloween storm” of October 1991 and the “storm of the century” of March 1993. J. Atmos. Ocean. Technol. 13, 198–230. https://doi.org/10.1175/1520-0426(1996)013<0198:EOCOWM>2.0.CO;2.

Cardone, V.J., Cox, A.T., 2009. Tropical cyclone wind field forcing for surge models: critical issues and sensitivities. Nat. Hazards 51, 29–47. https://doi.org/10.1007/s11069-009-9369-0.

Chan, K.T.F., Chan, J.C.L., 2015. Global climatology of tropical cyclone size as inferred from QuikSCAT data. Int. J. Climatol. 35 (15), 4843–4848. https://doi.org/10.1002/joc.4307.

Chao, Y.Y., Alves, J.G.M., Tolman, H.L., 2005. An operational system for predicting hurricane-generated wind waves in the North Atlantic Ocean. Weather Forecast. 20 (4), 652–671. https://doi.org/10.1175/WAF851.1.

Chao, Y.Y., Tolman, H.L., 2010. Performance of NCEP regional wave models in predicting peak sea states during the 2005 North Atlantic hurricane season. Weather Forecast. 25 (5), 1543–1567. https://doi.org/10.1175/2010WAF2222309.1.

Chavas, D.R., Knaff, J.A., 2022. A simple model for predicting the tropical cyclone radius of maximum wind from outer size. Weather Forecast. 37, 563–579. https://doi.org/10.1175/WAF-D-21-0103.1.

Chawla, A., Tolman, H.L., 2007. Automated grid generation for WAVEWATCH III. NOAA/NWS/ NCEP/OMB Tech. Note 254, 71.

Collins, C., Hesser, T., Rogowski, P., Merrifield, S., 2021. Altimeter Observations of Tropical Cyclone-generated Sea States: Spatial Analysis and Operational Hindcast Evaluation. J. Mar. Sci. Eng. 9, 216. https://doi.org/10.3390/jmse9020216.

Collins, C.O., Potter, H., Lund, B., Tamura, H., Graber, H.C., 2018. Directional wave spectra observed during intense tropical cyclones. J. Geophys. Res.-Ocean. 123, 773–779. https://doi.org/10.1002/2017JC012943.

Cox, A.T., Greenwood, J.A., Cardone, V.J., Swail, V.R., 1995. Wave hindcasting and forecasting: their role in ensuring the safety of personnel involved in offshore oil and gas exploitation. In: Proceedings of the 4th International Workshop on Wave Hindcasting and Forecasting, vols. 109–118. http://www.waveworkshop.org.

Donelan, M. A., et al., 1985. Directional Spectra of Wind-Generated Waves. *Philosophical Transactions of the Royal Society of London. Series A, Mathematical and Physical Sciences*, vol. 315, no. 1534, pp. 509–62. *JSTOR*. http://www.jstor.org/stable/37696.

Donelan, M.A., Babanin, A.V., Young, I.R., Banner, M.L., 2006. Wave-follower field measurements of the wind-input spectral function. Part II: parameterization of the wind input. J. Phys. Oceanogr. 36, 1672–1689. https://doi.org/10.1175/JPO2933.1.

Donelan, M.A., Curcic, M., Chen, S.S., Magnusson, A.K., 2012. Modeling waves and wind stress. J. Geophys. Res. 117, C00J23. https://doi.org/10.1029/2011JC007787.
Doyle, J.D., 2002. Coupled atmosphere–Ocean wave simulations under high wind conditions. Mon. Weather Rev. 130 (12), 3087–3099. https://doi.org/10.1175/1520-0493(2002)130<3087:CAOWSU>2.0.CO;2.
Emanuel, K.A., 1986. An air–sea interaction theory for tropical cyclones. Part 1: steady-state maintenance. J. Atmos. Sci. 43, 585–604. https://doi.org/10.1175/1520-0469(1986)043<0585:AASITF>2.0.CO;2.
Emanuel, K.A., 2000. A statistical analysis of tropical cyclone intensity. Mon. Weather Rev. 128 (4), 1139–1152. https://doi.org/10.1175/1520-0493(2000)128<1139:ASAOTC>2.0.CO;2.
Fan, Y., Ginis, I., Hara, T., Wright, C.W., Walsh, E.J., 2009. Numerical simulations and observations of surface wave fields under an extreme tropical cyclone. J. Phys. Oceanogr. 39 (9), 2097–2116. https://doi.org/10.1175/2009JPO4224.1.
Garg, N., Ng, E.Y.K., Narasimalu, S., 2018. The effects of sea spray and atmosphere–wave coupling on air–sea exchange during a tropical cyclone. Atmos. Chem. Phys. 18, 6001–6021. https://doi.org/10.5194/acp-18-6001-2018.
GEBCO Bathymetric Compilation Group, 2020. The GEBCO_2020 Grid - a Continuous Terrain Model of the Global Oceans and Land. British Oceanographic Data Centre, National Oceanography Centre, NERC, UK. https://doi.org/10.5285/a29c5465-b138-234d-e053-6c86abc040b9.
Group, T. W., 1988. The WAM Model—A Third Generation Ocean Wave Prediction Model. *J. Phys. Oceanogr.*, 18, 1775–1810. doi: 10.1175/1520-0485(1988)018<1775:TWMTGO>2.0.CO;2.
Haarsma, R.J., Roberts, M.J., Vidale, P.L., Senior, C.A., Bellucci, A., Bao, Q., Chang, P., Corti, S., Fučkar, N.S., Guemas, V., et al., 2016. High-resolution model intercomparison project (HighResMIP v1.0) for CMIP6. Geosci. Model Dev. 9, 4185–4208. https://doi.org/10.5194/gmd-9-4185-2016.
Hasselmann, D.E., Dunckel, M., Ewing, J.A., 1980. Directional wave spectra observed during JONSWAP 1973. J. Phys. Oceanogr. 10, 1264–1280. https://doi.org/10.1175/1520-0485(1980)010<1264:DWSODJ>2.0.CO;2.
Hasselmann, S., Hasselmann, K., 1985. Computations and parameterizations of the nonlinear energy transfer in a gravity wave spectrum, part 1: a new method for efficient computations of the exact nonlinear transfer integral. J. Phys. Oceanogr. 15, 1369–1377.
Hasselmann, S., Hasselmann, K., Allender, J.H., Barnett, T.P., 1985. Computations and parameterizations of the nonlinear energy transfer in a gravity wave spectrum, part 2: parameterizations of the nonlinear energy transfer for application in wave models. J. Phys. Oceanogr. 15, 1378–1391. doi:10.1175/1520-0485(1985)015<1378:CAPOTN>2.0.CO;2.
Hersbach, H., Bell, B., Berrisford, P., Hirahara, S., Horányi, A., Muñoz-Sabater, J., Nicolas, J., Peubey, C., Radu, R., Schepers, D., Simmons, A., 2020. The ERA5 global reanalysis. Q. J. R. Meteorol. Soc. 146 (730), 1999–2049. https://doi.org/10.1002/qj.3803.
Holland, G., 1980. An analytic model of the wind and pressure profiles in hurricanes. Mon. Weather Rev. 108, 1212–1218. doi:10.1175/1520-0493(1980)108<1212:AAMOTW>2.0.CO;2.
Holland, G., 2008. A revised hurricane pressure–wind model. Mon. Weather Rev. 136, 3432–3445. https://doi.org/10.1175/2008MWR2395.1.
Holland, G., Belanger, J.I., Fritz, A., 2010. A revised model for radial profiles of hurricane winds. Mon. Weather Rev. 138, 4393–4401. https://doi.org/10.1175/2010MWR3317.1.
Hu, K., Chen, Q., 2011. Directional spectra of hurricane-generated waves in the Gulf of Mexico. Geophys. Res. Lett. 38, L19608 https://doi.org/10.1029/2011GL049145.
Hu, K., Chen, Q., Kimball, S.K., 2012. Consistency in hurricane surface wind forecasting: an improved parametric model. Nat. Hazards 61, 1029–1105. https://doi.org/10.1007/s11069-011-9960-z.
Hu, Yuyi, Shao, Weizeng, Wei, Yongliang, Zuo, Juncheng, 2020. Analysis of typhoon-induced waves along typhoon tracks in the Western North Pacific ocean, 1998–2017. J. Mar. Sci. Eng. 8 (7), 521. https://doi.org/10.3390/jmse8070521.
Hwang, P.A., Fan, Y., 2017. Effective fetch and duration of tropical cyclone wind fields estimated from simultaneous wind and wave measurements: surface wave and air–sea exchange computation. J. Phys. Oceanogr. 47 (2), 447–470. https://doi.org/10.1175/JPO-D-16-0180.1.
Janssen, P.A.E.M., 1991. Quasilinear theory of wind-wave generation applied to wave forecasting. J. Phys. Oceanogr. 21, 1631–1642. https://doi.org/10.1175/1520-0485(1991)021<1631:QLTOWW>2.0.CO;2.
Kaiser, J., Nogueira, I.C.M., Campos, R.M., et al., 2022. Evaluation of wave model performance in the South Atlantic Ocean: a study about physical parameterization and wind forcing calibration. Ocean Dynam. 72, 137–150. https://doi.org/10.1007/s10236-021-01495-4.
Kalourazi, M.Y., Siadatmousavi, S.M., Yeganeh-Bakhtiary, A., Jose, F., 2021. WAVEWATCH-III source terms evaluation for optimizing hurricane wave modeling: a case study of Hurricane Ivan. Oceanologia 63 (2), 194–213. https://doi.org/10.1016/j.oceano.2020.12.001.
Kepert, J.D., 2012. Choosing a boundary layer parameterization for tropical cyclone modeling. Mon. Weather Rev. 140, 1427–1445. https://doi.org/10.1175/MWR-D-11-00217.1.
Kepert, J., Wang, Y., 2001. The dynamics of boundary layer jets within the tropical cyclone core. Part II: nonlinear enhancement. J. Atmos. Sci. 58, 2485–2501. https://doi.org/10.1175/1520-0469(2001)058<2485:TDOBLJ>2.0.CO;2.
King, D.B., Shemdin, O.H., 1978. Radar observations of hurricane wave directions. 16th Int. Conf. Coastal Eng. 209–226. https://doi.org/10.9753/icce.v16.10. Hamburg.
Klotz, B.W., Jiang, H., 2016. Global composites of surface wind speeds in tropical cyclones based on a 12-year scatterometer database. Geophys. Res. Lett. 43 https://doi.org/10.1002/2016GL071066, 10 480–10 488.
Knapp, K., Kruk, M., Levinson, D., Diamond, H., Neumann, C., 2010. THE international best track archive for climate stewardship (IBTrACS): unifying tropical cyclone data. Bull. Am. Meteorol. Soc. 91 (3), 363–376. http://www.jstor.org/stable/26232890.
Krien, Y., Arnaud, G., Cécé, R., Ruf, C., Belmadani, A., Khan, J., Bernard, D., Islam, A.K. M.S., Durand, F., Testut, L., Palany, P., Zahibo, N., 2018. Can we improve parametric cyclonic wind fields using recent satellite remote sensing data? Rem. Sens. 10 https://doi.org/10.3390/rs10121963, 1963.
Leckler, F., Ardhuin, F., Filipot, J.F., Mironov, A., 2013. Dissipation source terms and whitecap statistics. Ocean Model. 70, 62–74. https://doi.org/10.1016/j.ocemod.2013.03.007.
Lee, C., Chen, S.S., 2012. Symmetric and asymmetric structures of hurricane boundary layer in coupled atmosphere–wave–ocean models and observations. J. Atmos. Sci. 69 (12), 3576–3594. https://doi.org/10.1175/JAS-D-12-046.1.
Liu, Q., Babanin, A., Fan, Y., Zieger, S., Guan, C., Moon, I.J., 2017. Numerical simulations of ocean surface waves under hurricane conditions: assessment of existing model performance. Ocean Model. 118, 73–93. https://doi.org/10.1016/j.ocemod.2017.08.005.
Liu, Q., Rogers, W.E., Babanin, A.V., Young, I.R., Romero, L., Zieger, S., Qiao, F., Guan, C., 2019. Observation-based source terms in the third-generation wave model WAVEWATCH III: updates and verification. J. Phys. Oceanogr. 49 (2), 489–517. https://doi.org/10.1175/JPO-D-18-0137.1.
Ma, Z., Zhao, C., Gong, J., Zhang, J., Li, Z., Sun, J., Liu, Y., Chen, J., Jiang, Q., 2021. Spin-up characteristics with three types of initial fields and the restart effects on forecast accuracy in the GRAPES global forecast system. Geosci. Model Dev. 14, 205–221. https://doi.org/10.5194/gmd-14-205-2021.
McConochie, J.D., Hardy, T.A., Mason, L.B., 2004. Modelling tropical cyclone over-water wind and pressure fields. Ocean Eng. 31 (Issues 14–15), 1757–1782. https://doi.org/10.1016/j.oceaneng.2004.03.009.
Mok, D.K.H., Chan, J.C.L., Chan, K.T.F., 2018. A 31-year climatology of tropical cyclone size from the NCEP Climate Forecast System Reanalysis. Int. J. Climatol. 38, e796–e806. https://doi.org/10.1002/joc.5407.
Moon, I.J., Ginis, I., Hara, T., et al., 2003. Numerical simulation of sea surface directional wave spectra under Hurricane wind forcing. J. Phys. Oceanogr. 33 (8), 1680–1706. https://doi.org/10.1175/2410.1.
Ochi, M.K., 1993. On hurricane-generated seas. In: Proc. Second Int. Symp. On Ocean Wave Measurement and Analysis, pp. 374–387. New Orleans, LA, ASCE.
Olfateh, M., Callaghan, D.P., Nielsen, P., Baldock, T.E., 2017. Tropical cyclone wind field asymmetry - development and evaluation of a new parametric model. J. Geophys. Res. Oceans. 122, 458–469. https://doi.org/10.1002/2016JC012237.
Powell, M.D., 1982. The transition of the Hurricane Frederic boundary-layer wind field from the open Gulf of Mexico to landfall. Mon. Weather Rev. 110, 1912–1932. https://doi.org/10.1175/1520-0493(1982)110<1912:TTOTHF>2.0.CO;2.
Powell, M., Houston, S., Amat, L., Morisseau-Leroy, N., 1998. The HRD real time hurricane wind analysis system. J. Wind Eng. Ind. Aerod. 77–78, 53–64. https://doi.org/10.1016/S0167-6105%2898%2900131-7.
Rascle, N., Ardhuin, F., 2013. A global wave parameter data base for geophysical applications. Part 2: model validation with improved source term parameterization. Ocean Model. 70, 174–188. https://doi.org/10.1016/j.ocemod.2012.12.001.
Ribal, A., Young, I.R., 2020. Calibration and cross-validation of global ocean wind speed based on scatterometer observations. J. Atmos. Ocean. Technol. 37, 279–297. https://doi.org/10.1175/JTECH-D-19-0119.1.
Roberts, M.J., Camp, J., Seddon, J., Vidale, P.L., Hodges, K., Vanniere, B., Mecking, J., Haarsma, R., Bellucci, A., Scoccimarro, E., et al., 2020. Impact of model resolution on tropical cyclone simulation using the HighResMIP–PRIMAVERA multimodel ensemble. J. Clim. 33, 2557–2583. https://doi.org/10.1175/JCLI-D-19-0639.1.
Rogers, E., Babanin, A., Wang, D., 2012. Observation consistent input and whitecapping dissipation in a model for wind-generated surface waves: description and simple calculations. J. Atmos. Oceanic Tech. 29 (9), 1329–1346. https://doi.org/10.1175/JTECH-D-11-00092.1.
Ruiz-Salcines, P., Salles, P., Robles-Díaz, L., Díaz-Hernández, G., Torres-Freyermuth, A., Appendini, C.M., 2019. On the use of parametric wind models for wind wave modeling under tropical cyclones. Water 11, 2044. https://doi.org/10.3390/w11102044.
Saha, S., et al., 2010. The NCEP climate forecast system reanalysis. Bull. Am. Meteorol. Soc. 91 (8), 1015–1058. https://doi.org/10.1175/2010BAMS3001.1.
Shao, W.Z., Hu, Y.Y., Yang, J.S., Nunziata, F., Sun, J., Li, H., Zuo, J.C., 2018. An empirical algorithm to retrieve significant wave height from Sentinel-1 synthetic aperture radar imagery collected under cyclonic conditions. Rem. Sens. 10, 1367. https://doi.org/10.3390/rs10091367.
Shapiro, L.J., 1983. The asymmetric boundary layer under a translating hurricane. J. Atmos. Sci. 40, 1984–1998. https://doi.org/10.1175/1520-0469(1983)040<1984:TABLFU>2.0.CO;2.
Shapiro, L.J., Willoughby, H.E., 1982. The response of balanced hurricanes to local sources of heat and momentum. J. Atmos. Sci. 39, 378–394. https://doi.org/10.1175/1520-0469(1982)039<0378:TROBHT>2.0.CO;2.
Shea, D.J., Gray, W.M., 1973. The hurricanes's inner core region: symmetric and asymmetric structure. J. Atmos. Sci. 30, 1544–1564. https://doi.org/10.1175/1520-0469(1973)030<1544:THICRI>2.0.CO;2.
Shemdin, O.H., 1977. Hurricane Waves, Storm Surge and Currents: an Assessment of the State of the Art, US-South East Asia Symp. on Eng. for Natural Hazards Protection, Manila.
Soran, M.B., Amarouche, K., Akpınar, A., 2022. Spatial calibration of WAVEWATCH III model against satellite observations using different input and dissipation parameterizations in the Black Sea. Ocean Eng. 257, 111627 https://doi.org/10.1016/j.oceaneng.2022.111627.

Stopa, J.E., Ardhuin, F., Babanin, A., Zieger, S., 2016. Comparison and validation of physical wave parameterizations in spectral wavemodels. Ocean Model. 103, 2–17. Waves and coastal, regional andglobal processes.
Strachan, J., Vidale, P.L., Hodges, K., Roberts, M., Demory, M.-E., 2013. Investigating global tropical cyclone activity with a hierarchy of AGCMs: the role of model resolution. J. Clim. 26, 133–152. https://doi.org/10.1175/JCLI-D-12-00012.1.
Surgi, N., Pan, H., Lord, S.J., 1998. Improvement of the NCEP global model over the tropics: an evaluation of model performance during the 1995 hurricane season. Mon. Weather Rev. 126 (5), 1287–1305. https://doi.org/10.1175/1520-0493(1998)126<1287:IOTNGM>2.0.CO;2.
Tamizi, A., Young, I.R., 2020. The spatial distribution of ocean waves in tropical cyclones. J. Phys. Oceanogr. 50, 2123–2139. https://doi.org/10.1175/JPO-D-20-0020.1.
Tamizi, A., Young, I.R., Ribal, A., Alves, J.-H., 2020. Global scatterometer observations of the structure of tropical cyclone wind fields. Mon. Weather Rev. 148, 4673–4692. https://doi.org/10.1175/MWR-D-20-0196.1.
Tamizi, A., Alves, J., Young, I.R., 2021. The physics of Ocean wave evolution within tropical cyclones. J. Phys. Oceanogr. 51 (7), 2373–2388. https://doi.org/10.1175/JPO-D-21-0005.1.
Thomsen, G.L., Smith, R.K., Montgomery, M.T., 2015. Tropical cyclone flow asymmetries induced by a uniform flow revisited. J. Adv. Model. Earth Syst. 7, 1265–1284. https://doi.org/10.1002/2015MS000477.
Tolman, H.L., 1997. User Manual and System Documentation of WAVEWATCH-III Version 1.15, vol. 151. NOAA/NWS/NCEP/OMB Technical Note, p. 97.
Tolman, H.L., 1999. User Manual and System Documentation of WAVE-WATCHIII version 1.18, vol. 166. NOAA/NWS/NCEP/OMB technical note, p. 100, 1999.
Tolman, H.L., 2002. User Manual and System Documentation of WAVEWATCH III Version 2.22. Tech. Note 222. NOAA/NWS/NCEP/MMAB, p. 133.
Tolman, H.L., 2009. User Manual and System Documentation of WAVEWATCH III Version 3.14, vol. 276. NOAA/NWS/NCEP/MMAB Technical Note, p. 194. + Appendices.
Tolman, H.L., 2010. WAVEWATCH III r development best practices. NOAA/NWS / NCEP / MMAB Technical Note 286, 26.
Tolman, H.L., 2014. User manual and system documentation of WAVEWATCH III version 4.18. NOAA/NWS/NCEP/MMAB. Technical Note 316, 194.
Tolman, H.L., Alves, J.-H.G.M., 2005. Numerical modeling of wind waves generated by tropical cyclones using moving grids. Ocean Model. 9 (4), 305–323. https://doi.org/10.1016/j.ocemod.2004.09.003.
Tolman, H.L., Alves, J.-H.G.M., Chao, Y.Y., 2005. Operational forecasting of wind-generated waves by hurricane isabel at NCEP. Weather Forecast. 20, 544–557. https://doi.org/10.1175/WAF852.1.
Tolman, H.L., Chalikov, D., 1996. Source terms in a third-generation wind wave model. J. Phys. Oceanogr. 26, 2497–2518. https://doi.org/10.1175/1520-0485(1996)026<2497:STIATG>2.0.CO;2.
Uhlhorn, E.W., Klotz, B., Vukicevic, W.T., Easor, P.D.R., Rogers, R.F., 2014. Observed hurricane wind speed asymmetries and relationships to motion and environmental shear. Mon. Weather Rev. 142, 1290–1311. https://doi.org/10.1175/MWR-D-13-00249.1.
Varlas, G., Vervatis, V., Spyrou, C., Papadopoulou, E., Papadopoulos, A., Katsafados, P., 2020. Investigating the impact of atmosphere-wave-ocean interactions on a Mediterranean tropical-like cyclone. Ocean Model. 153, 101675 https://doi.org/10.1016/j.ocemod.2020.101675.
Vickery, P.J., Wadhera, D., 2008. Statistical models of Holland pressure profile parameter and radius to maximum winds of hurricanes from flight-level pressure and H*wind data. J. Appl. Meteorol. Climatol. 47, 2497–2517. https://doi.org/10.1175/2008JAMC1837.1.
Walsh, E.J., Wright, C.W., Vandemark, D., Krabill, W.B., Garcia, A.W., Houston, S.H., Murillo, S.T., Powell, M.D., Black, P.G., Marks Jr., F.D., 2002. Hurricane directional wave spectrum spatial variation at landfall. J. Phys. Oceanogr. 32 (6), 1667–1684.
Wehner, M.F., Reed, K.A., Li, F., Bacmeister, J., Chen, C.-T., Paciorek, C., Gleckler, P., Sperber, K., Collins, W.D., Andrew, G., et al., 2014. The effect of horizontal resolution on simulation quality in the Community Atmospheric Model, CAM5.1. J. Adv. Model. Earth Syst. 6, 980–997.
Wessel, P., Smith, W.H.F., 1996. A global, self-consistent, hierarchical, high-resolution shoreline database. J. Geophys. Res. 101, 8741–8743. https://doi.org/10.1029/96JB00104.
Willoughby, H.E., Darling, R.W.R., Rahn, M.E., 2006. Parametric representation of the primary hurricane vortex. Part II: a new family of sectionally continuous profiles. Mon. Weather Rev. 134, 1102–1120. https://doi.org/10.1175/MWR3106.1.
Wright, C.W., Walsh, E.J., Vandemark, D., Krabill, W.B., Garcia, A.W., Houston, S.H., Powell, M.D., Black, P.G., Marks, F.D., 2001. Hurricane directional wave spectrum spatial variation in the open ocean. J. Phys. Oceanogr. 31 (8), 2472–2488.
WW3DG, 2019. WAVEWATCH III® Development Group, p. 326. User manual version 6.07. Tech. Note 333, NOAA/NWS/NCEP/MMAB, USA.
Yang, H., Shao, Z., Liang, B., Wang, Z., Lee, D., 2022. Performance of different input and dissipation packages in WAVEWATCH III model during tropical cyclones. Phys. Fluids 34, 107102.
Young, I.R., 1988. A parametric hurricane wave prediction model. J. Waterw. Port, Coast. Ocean Eng. 114 (5), 637–652. https://doi.org/10.1061/(ASCE)0733-950X.
Young, I.R., 2006. Directional spectra of hurricane wind waves. J. Geophys. Res. 111, C08020 https://doi.org/10.1029/2006JC003540.
Young, I.R., 2017. A review of parametric descriptions of tropical cyclone wind-wave generation. Atmosphere 8 (10), 194. https://doi.org/10.3390/atmos8100194.
Young, I., Burchell, G., 1996. Hurricane generated waves as observed by satellite. Ocean Eng. 23, 761–776. https://doi.org/10.1016/0029-8018(96)00001-7.
Young, I., Babanin, A., 2006. Spectral distribution of energy dissipation of wind generated waves due to dominant wave breaking. J. Phys. Oceanogr. 36 (3), 376–394. https://doi.org/10.1175/JPO2859.1.
Young, I.R., Vinoth, J., 2013. An 'extended fetch' model for the spatial distribution of tropical cyclone wind–waves as observed by altimeter. Ocean Eng. 70, 14–24. https://doi.org/10.1016/j.oceaneng.2013.05.015.
Young, I.R., Fontain, E., Liu, Q., Babanin, A.V., 2020. The wave climate of the Southern Ocean. J. Phys. Oceanogr. 50, 1417–1433. https://doi.org/10.1175/JPO-D-20-0031.1.
Zhao, B., Qiao, F., Cavaleri, L., Wang, G., Bertotti, L., Liu, L., 2017. Sensitivity of typhoon modeling to surface waves and rainfall. J. Geophys. Res. Ocean. 122, 1702–1723. https://doi.org/10.1002/2016JC012262, 2017.
Zhang, J., Uhlhorn, E.W., 2012. Hurricane sea surface inflow angle and an observation-based parametric model. Mon. Weather Rev. 140, 3587–3605. https://doi.org/10.1175/MWR-D-11-00339.1.
Zhang, L., Liu, G., Perrie, W., He, Y., Zhang, G., 2018. Typhoon/hurricane-generated wind waves inferred from SAR imagery. Rem. Sens. 10, 1605. https://doi.org/10.3390/rs10101605.
Zieger, S., Babanin, A., Rogers, W., Young, I., 2015. Observation-based source terms in the third-generation wave model WAVEWATCH. Ocean Model. 96 (Pt.1), 2–25. https://doi.org/10.1016/j.ocemod.2015.07.014.
Zieger, S., Greenslade, D.J.M., Aijaz, S., Kepert, J.D., Burton, A., 2021a. Hindcasting of tropical cyclone winds and waves. Ocean Dynam. 71, 559–588. https://doi.org/10.1007/s10236-021-01443-2.
Zieger, S., Kepert, J.D., Greenslade, D.J.M., Aijaz, S., 2021b. Assessment of tropical cyclone wave models for engineering applications. Ocean Eng. 225, 108748 https://doi.org/10.1016/j.oceaneng.2021.108748.